Tunable Semiconductor Lasers: A Tutorial

Larry A. Coldren, *Fellow, IEEE*, G. A. Fish, Y. Akulova, J. S. Barton, L. Johansson, and C. W. Coldren, *Member, IEEE*

Tutorial Paper

***Abstract*—Tunable semiconductor lasers have been listed in numerous critical technology lists for future optical communication and sensing systems. This paper summarizes a tutorial that was given at OFC '03. It includes some discussion of why tunable lasers might be beneficial, an outline of basic tuning mechanisms, some examples of tunable lasers that have been commercialized, and a discussion of control techniques. More extensive data is given for the widely-tunable sampled-grating distributed-Bragg-reflector (SGDBR) type of laser, including data for such lasers integrated monolithically with modulators to form complete transmitter front ends. A summary of reliability data for the SGDBR laser is also given. It is concluded that tunable lasers can reduce operational costs, that full-band tunability is desirable for many applications, that monolithic integration offers the most potential for reducing size, weight, power and cost, and that sufficient reliability for system insertion has been demonstrated.**

***Index Terms*—Photonic integrated circuits, semiconductor lasers, tunable lasers.**

I. Introduction

TUNABLE lasers have been of interest for some time [1]. Applications range from sources for fiber optic telecommunication systems to broadband sensors. About three or four years ago, the telecom application began to drive significant investments into this field to support the perceived need for dynamic networks and wavelength reconfigurability in wavelength division multiplexing (WDM) systems. Vast reductions in operational costs were predicted for such flexible fiber-optic networks that were thought to be necessary for the rapidly expanding demand for bandwidth. However, as many new companies joined this effort, there was a large overbuild of capacity, and the need for the new networks vanished, or more accurately, was pushed back to least the present time. The good news for the industry is that the demand for bandwidth continues to nearly double each year.

Although the potential to reduce operational costs with more dynamical networks still exists, the delay in significant network expansion has led to a reappraisal of the value proposition for tunable lasers. Today, the main value for telecom networks appears to be in the areas of inventory reduction, both in the manufacture and operation of WDM systems. With fixed frequency distributed-feedback (DFB) lasers, dozens of different wavelength codes must be manufactured and inventoried, and perhaps more importantly, dozens of different wavelength-specific line cards must be manufactured and inventoried. Since the cost of line cards is measured in multiples of $10 k, this can be a significant overhead. Thus, even for this less glamorous application, the savings are finite, but as a result, today's tunable laser solutions are compared to fixed-frequency DFBs for both cost and performance.

Bearing all of this in mind, it is generally agreed that if tunable lasers with the same performance specs as DFBs were available, most systems companies would select them over DFBs for a small price premium. As we will show in this report, some tunable embodiments appear to have reached specification parity with DFBs, so the situation may indeed be favorable for tunables in future WDM networks. By the time one considers the price of a line card, the increased cost of incorporating the tunable laser can be quite small, relatively speaking, and one can gain the functionality of a "universal" line card, which can be programmed to function at any wavelength over the tuning range of the laser [2]. Of course, this is a strong argument for full-band tunability in the laser, because only one part would then be necessary for any slot. Finally, there is still the compelling argument that the line card can be re-provisioned at some later point in time, should the network architecture evolve to accommodate this, and again, full-band tunability would be desired.

The situation in the sensor area is perhaps even more attractive for tunable lasers. Here many sensor types rely upon the ability to sweep the laser frequency over a wide range for their basic functionality, so they are essential. This, perhaps, is a subject for a different audience than those attending the Optical Fiber Communication conference, the audience for which this tutorial was designed.

II. Why Tunable Lasers?

Although we have already stated that the current justification for wanting tunable laser solutions is in reduced manufacturing and operational costs deriving from inventory reduction, there are still a number of potential applications in the telecom area that might be important in the near future [3]. The first to be mentioned is in reconfigurable optical-add-drop multiplexers (ROADMs). As illustrated in Fig. 1 these allow single (or multiple) optical channels to be removed and replaced on a fiber without de-multiplexing, regenerating, and re-multiplexing the entire array of wavelengths contained in the fiber. In applications where this functionality is desired, the ROADM can vastly reduce the cost of dropping and/or adding a relatively small amount of information from or to the fiber.

Manuscript received July 2, 2003; revised October 10, 2003.

L. A. Coldren is with the Departments of Materials and Electrical & Computer Engineering, University California, Santa Barbara, CA 93106 USA, and is also with the Agility Communications, Incorporated, Santa Barbara, CA 93117 USA.

G. A. Fish, Y. Akulova, and C. W. Coldren are with the Agility Communications, Incorporated, Santa Barbara, CA 93117 USA.

J. S. Barton and L. Johansson are with the Departments of Materials and Electrical & Computer Engineering, University California, Santa Barbara, CA 93106 USA.

Digital Object Identifier 10.1109/JLT.2003.822207

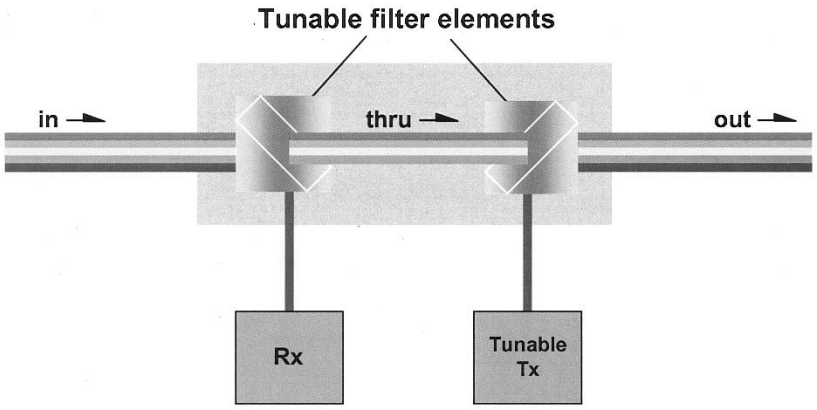

Fig. 1. Reconfigurable optical add/drop port. A tunable filter selectively removes (or adds) a single (or several) optical WDM channel from the fiber. A tunable transmitter is needed to insert any desired channel at the add port.

Tunable lasers are also natural complementary components in optical switches of various kinds. Here they generally are used for the function of wavelength switching or "wavelength conversion," in which an incoming signal on one wavelength is remodulated onto another wavelength on the output [4]. This can be accomplished in numerous ways, the most straightforward of which is to incorporate a tunable laser within a line card or transponder, so that the output can be set to any wavelength value. These "optical-electronic-optical" (OEO) components include 3R regeneration to reconstitute the signal to its original form. One can also make "all optical" wavelength converters that use the incoming signal on one wavelength to drive a modulator that applies the signal directly to a second selectable output wavelength generated by a tunable laser. Recently, this function has been demonstrated with a single monolithic chip [5], [6]. However, in these "all-optical" approaches 3R or even 2R regeneration of the signal is generally not provided, so that these elements can only work with relatively clean data, and they can only be cascaded a few times before a 3R regeneration is necessary.

Fig. 2 shows an all-optical space switch that uses wavelength converters at the input and a passive optical router switching fabric to provide space switching. In this case the input signal is placed on the wavelength that the passive "lambda router" will route to the desired output port. If the signal is to be re-mutiplexed, it would then have to be again converted to the desired wavelength to enter the optical multiplexer. This sort of switching architecture is also currently being investigated by several groups for all-optical packet switching [7], [8]. In this case, the tunable lasers in the front-end wavelength converters (shown as line cards with tunable lasers in Fig. 2) must switch wavelengths very fast—typically in the nanosecond range. Such a criterion will favor the tunable laser types that are controlled electronically versus the ones that have thermal or mechanical tuning elements.

Again, the sensor application area has already been mentioned, so it shall not be discussed further here.

III. Basic Tuning Mechanisms

Fig. 3 gives a schematic of a generic tunable laser together with the relative spectra of the necessary filter and gain elements as well as the location of the various cavity modes that all must be properly aligned and translated to create a tunable, single-frequency laser. Of course, in most practical embodiments, the

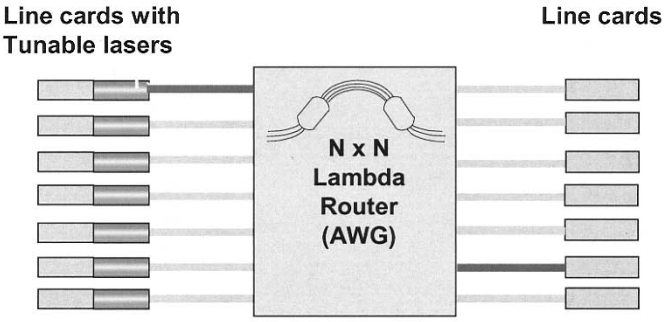

Fig. 2. Transparent optical space switch composed of a wavelength converter array and a passive router such as an arrayed-waveguide-router (AWG). Line cards with tunable lasers can more generally be replaced by wavelength converters.

filter, mirror and phase-shifting elements are combined in some way to create a unique physical structure for the different kinds of tunable lasers. Fig. 3 can be used to see how a tunable semiconductor laser evolves from the most basic "Fabry-Perot" laser, which has just the gain and the two simple mirror elements, to a "single-frequency" laser, which adds the mode-selection filter, to a "tunable single-frequency" laser, which adds possible adjustment of the mirror position and the center frequency of the mode-selection filter, as well as adding a new adjustable cavity phase element. For more analytical discussion, the reader is referred to [9], [10].

The most common Fabry-Perot laser is composed of a uniform cleaved semiconductor chip that is structured to provide gain for a guided optical mode with the cleaves functioning as the mirrors. The most common single-frequency laser is probably the DFB laser, illustrated in Fig. 4(a), in which an index grating is formed near the optical waveguide to provide a continuous reflection that gives both the mirror functionality as well as the mode selection filter. The vertical-cavity surface-emitting laser (VCSEL) as illustrated in Fig. 4(b), is also a single-frequency laser, but in this case the cavity is vertical and the grating mirrors sandwich the gain region. Although the distributed-Bragg-reflector (DBR) mirrors are frequency selective, the primary mode selection is done by the finite width of the gain spectrum in this case, because both the mirror spectrum and the mode spacing are made large by the short cavity length—a somewhat different case than that suggested in Fig. 3.

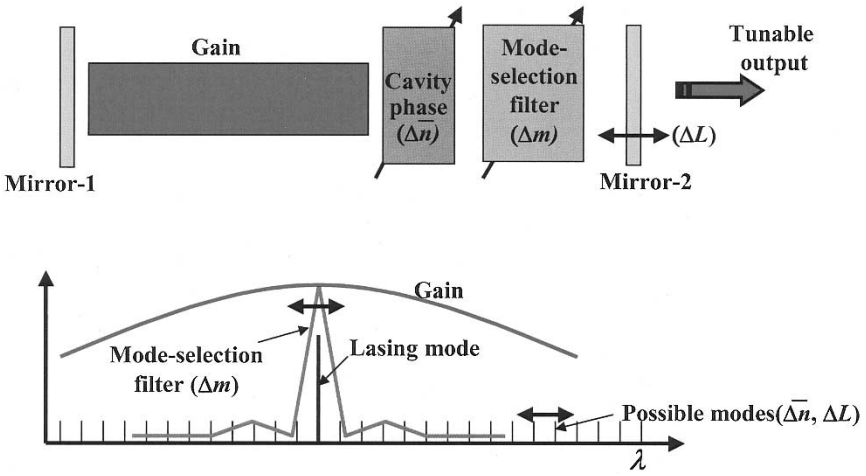

Fig. 3. Schematic of generic tunable laser together with relationship of the spectra of each element.

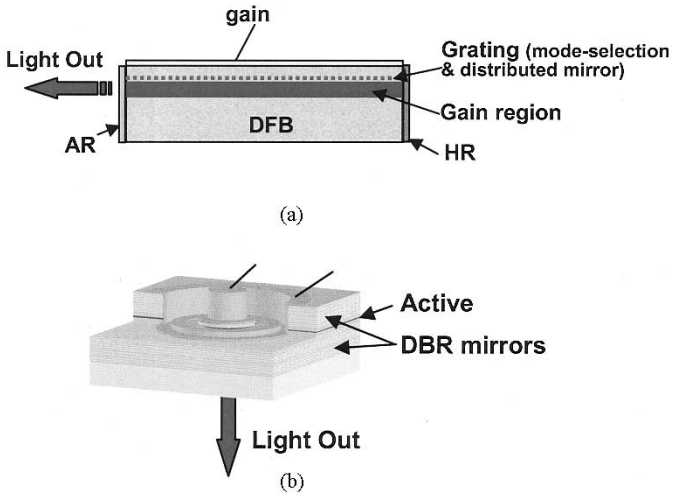

Fig. 4. Examples of single-frequency lasers (not tunable): (a) DFB laser and (b) VCSEL.

Equation (1) gives the relationship between the lasing wavelength, λ, and the cavity mode number, m, effective index of refraction seen by the cavity mode, $\bar{n}$, and the effective cavity length, L. Quite obviously, if one changes m, $\bar{n}$, or L, the wavelength must also change. The relative change in wavelength derived from (1) is given in (2). As indicated the relative wavelength change is directly proportional to the relative change in either the length, index or mode number

Mode number — Effective cavity length

$$\frac{m\lambda}{2} = \bar{n}L \tag{1}$$

Wavelength — Effective index

Tuned by mode-selection filter (via index or grating angle)

$$\frac{\Delta\lambda}{\lambda} = \frac{\Delta\bar{n}}{\bar{n}} + \frac{\Delta L}{L} - \frac{\Delta m}{m} \tag{2}$$

Tuned by net cavity index change — Tuned by physical length change

IV. Examples of Tunable Semiconductor Lasers

Fig. 5 shows several different types of tunable single-frequency lasers that have been commercialized. (Since tunable lasers need to be single frequency to be of much use, we will now drop this qualifier.) In the figure we have only included the widely-tunable varieties that are capable of full *C* or *L*-band coverage from a single device.

The first example shows a selectable array of DFB lasers that are combined in a multimode interference coupler. The DFBs are excited one at a time and each is manufactured with a slightly different grating pitch to offset their output wavelengths by about 3 or 4 nm. The chip is then temperature tuned by some 30–40 C to access the wavelengths between the discrete values of the array elements. With N-DFB elements, then, a wavelength range of up to about $4N$ nm can be accessed, or with 8–10 elements the entire *C*-band can be accessed. The schematic included in Fig. 5(a) is from NEC[11]; however, similar work is also being carried out at Fujitsu [12] and other mostly Japanese labs. Santur Corporation uses a similar concept, but with an external micro-electromechanical (MEMs) mirror to select which element is coupled to the output fiber [13], thus eliminating the $1/N$ combiner loss, but at the expense of one more element to package and control. In all cases, this approach must deal with the requirement of having a number of closely spaced DFBs all working to tight specifications. The losses in combining, inherent in most varieties, are also significant, and the need to temperature tune over a fairly large tuning range leads to relatively high power dissipation for this approach.

Fig. 5(b) is an example of an external-cavity laser. In this case a "gain block" is coupled to external mode-selection filtering and tuning elements via bulk optical elements. The cavity phase adjustment, necessary to properly align the mode with the filter peak and the desired ITU grid wavelength, can be included in one of several places—e.g., on the gain block or by fine tuning the mirror position. In most external-cavity approaches the mode selection filter is a diffraction grating that can also double as a mirror. The so-called Littman-Metcalf cavity arrangement is illustrated. In this case, a retro-reflecting mirror is translated as it is rotated. This combined motion changes the ef-

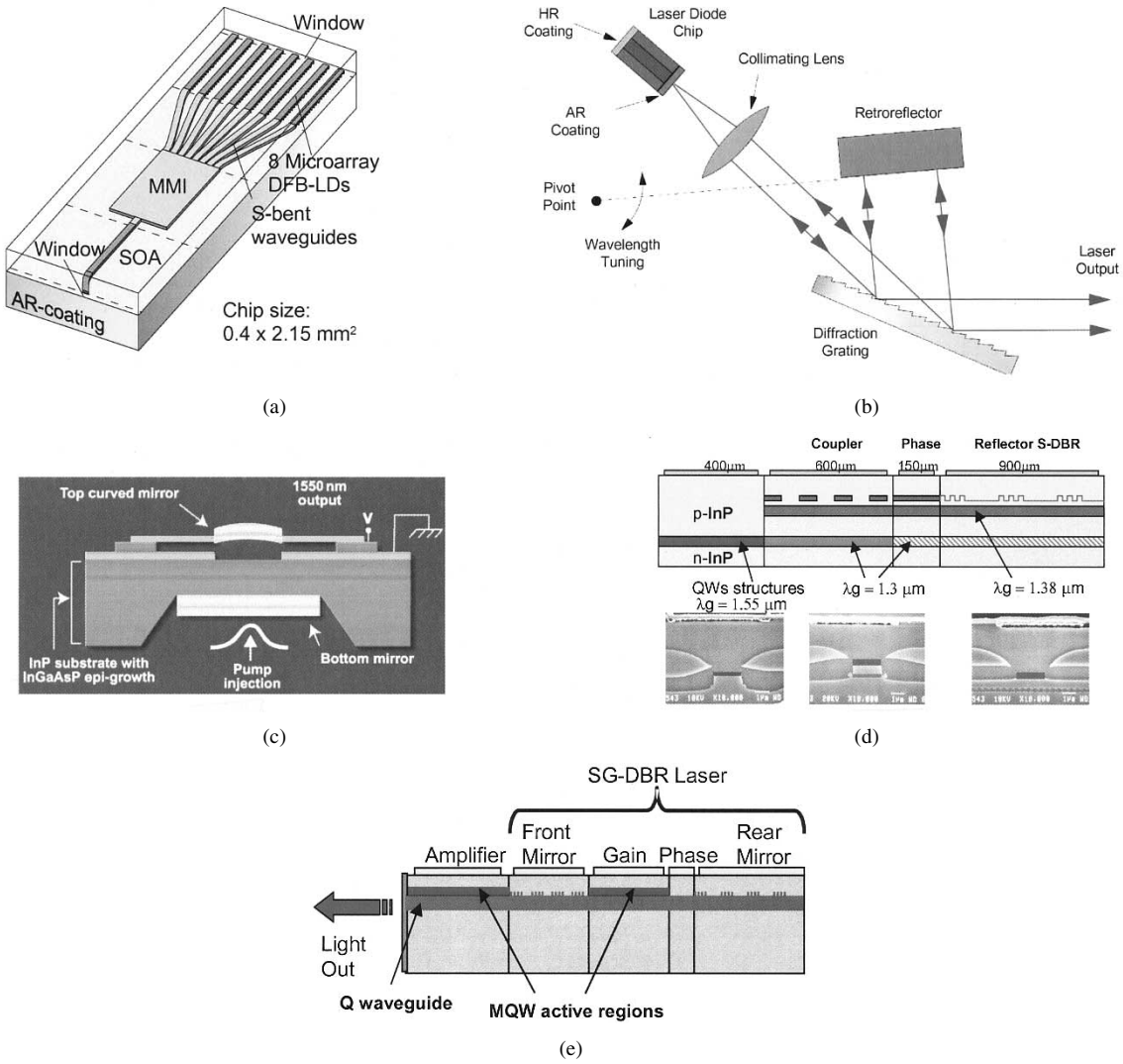

Fig. 5. Examples of widely-tunable laser types: (a) selectable DFB array, (b) external-cavity, (c) MEMs/VCSEL, (d) grating-coupled sampled-reflector (GCSR), and (e) sampled-grating DBR (SGDBR) with integrated SOA.

fective cavity length in proportion to the change in center wavelength of the mode-selection filter to track the movement of a single cavity mode. The Littman-Metcalf geometry provides continuous tuning over some range, but due to cavity dispersion, one in general still needs to correct the cavity phase at each ITU channel. This approach has been used by Iolon [14] and New Focus [15] in their products. Other companies tend to just rotate the mirror and let the mode selection filter scan across the modes. This is most common in scientific instruments, where the cavities are quite long and the mode spacing very small. Intel also has reported some research [16] in which the external cavity contains two temperature-tuned etalons with slightly different resonance frequencies, which act in combination to create a widely-tunable filter. A standard external mirror completes the cavity. All of the external cavity approaches appear to provide useable specs for telecommunications, although at this writing we are not aware of any that has completed the full Telcordia qualification exercise. An obvious concern with these structures is their manufacturability and reliability, given the need for assembling numerous micro-optical parts and holding them in precise alignment.

Fig. 5(c) shows a tunable VCSEL that is created by mounting one mirror on a flexible arm and using an electrostatic force to translate it up and down. This MEMs approach has been employed by Coretek [17]—later acquired by Nortel—[as shown in Fig. 5(c)] and Bandwidth 9 [18]. In Coretek's case external optical pumping was used, and in Bandwidth 9's case electrical pumping was employed. Both efforts appear to have been discontinued. The Coretek approach used dielectric mirrors for wide reflection bandwidth. Thus, it was able to show full *C*-band operation; the Bandwidth 9 device had a somewhat smaller tuning range. The use of optical pumping also provides for more power output, although advertised products from Nortel did include an external amplifier to boost the fiber-coupled power to the 20 mW range. A primary appeal for the VCSEL approaches is the wafer-scale manufacturing platform that it appears to provide. The hope here was to make tunable devices for nearly the same cost as the 850 nm VCSELs used in Gigabit Ethernet. However, at 1550 nm VCSEL construction is more difficult, and limited output power together with wide optical linewidth appear to be serious limitations with the VCSEL approaches at 1550 nm.

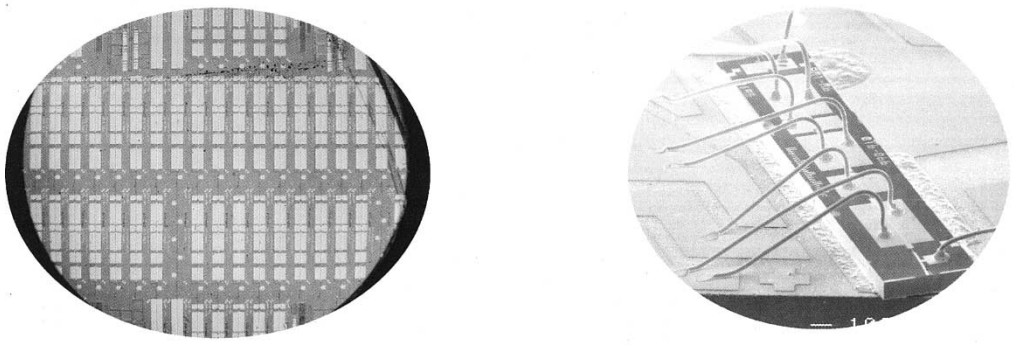

(a) (b)

Fig. 6. Photo of wafer and SEM of mounted single-chip transmitter.

Fig. 5(d) and (e) show monolithic widely-tunable semiconductor laser approaches that employ electronic tuning of the index in a single cavity to provide for full *C*- or *L*-band wavelength coverage. Both are variations on older DBR laser approaches [19]–[21], but both employ concepts to tune the relative wavelength by up to an order of magnitude more than the index of any section can be tuned. In the case of Fig. 5(d), the so-called grating-coupled sampled-reflector (GCSR) laser [22], [23], this is accomplished by using a property of a grating-assisted co-directional coupler which has a tuning proportional to the index tuning relative to the *difference* in index between two coupled waveguides, $\Delta n/(n_1 - n_2)$, rather than $\Delta n/n_1$ as in most other filters. However, because the filter is also broad, a back multiple-order sampled-grating reflector is required for good mode selectivity in this case. In the SGDBR of Fig. 5(e) [24], [25], the wider tuning range filter is provided by the product of the two differently spaced and independently tuned reflection combs of the SGDBRs at each end of the cavity. This product, R_1R_2, is what appears in the laser cavity loss factors, and the variation in the beating effect between the two different mirror reflection combs is sometimes referred to as the vernier effect. In this case the net mode selection filter wavelength tuning is that of a single grating, $\Delta n/n$, multiplied by $\delta\lambda/\Delta\lambda$, the difference in spacing between the mirror reflection peaks of the two mirrors, $\delta\lambda$, divided by the mean mirror peak spacing, $\Delta\lambda$. Similar physics is involved in the superstructure-grating DBR developed at NTT [26]. In both cases, good side-mode suppression has been demonstrated, and tuning of over 40 nm is easily accomplished, but due to grating losses resulting from current injection for tuning, the differential efficiency and chip output powers can be somewhat limited. In the case of the SGDBR, this is easily addressed by the incorporation of another gain section on the output side of the output mirror, and fiber-coupled powers of up to 40 mW have been reported. In fact, this is the embodiment illustrated in Fig. 5(e). Incorporating such a semiconductor-optical-amplifier (SOA) is not as easy for the GCSR, so fiber-coupled powers of typically less than 10 mW result. The integrated SOA also has other benefits for the SGDBR as will be discussed in the following.

V. Characteristics of SGDBR Lasers and Single-Chip Transmitters

Work at UCSB and Agility Communications has aimed to develop widely tunable lasers and transmitters with monolithically integrated modulators. A low-cost "platform technology" that is capable of providing a wide variety of photonic ICs (PICs) without changing the basic manufacturing process has been developed. Fig. 6 shows a photograph of a $2''$ InP wafer with arrays of seven-section photonic IC transmitters, each consisting of a full-band-tunable four-section SGDBR laser integrated with a monitoring detector, optical amplifier, and modulator. The SEM inset shows one of these mounted on a carrier ready to be inserted into a package. It is important to note that the wafer layer structure and processing procedure used is identical to that developed for the SGDBR laser alone. This same structure and processing procedure is also used in the more complex laser PICs to be discussed below. Note also a key advantage of photonic integration—only one optical coupling to fiber is required, as would be necessary for a simple DFB laser alone.

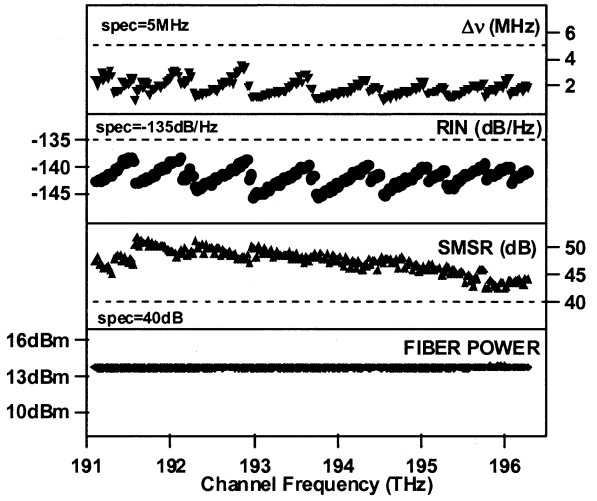

Fig. 7. CW characteristics of SGCBR-SOA device for 100 channels—calibrated for 20 mW of fiber power. The linewidth, $\Delta\nu$, relative intensity noise, RIN, and side-mode suppression ratio, SMSR shown for all *C*-band channels.

The basic SGDBR-SOA shown in Fig. 5(e) above as well as the integrated SGDBR-SOA-EAM transmitter illustrated in Fig. 6 have been productized and Telcordia qualified for telecom applications [27]. In Fig. 7 we give a summary of the characteristics of a 20 mW cw product similar to Fig. 5(e) at each of 100 channels spaced by 50 GHz across the *C*-band. A common quaternary waveguide extends throughout the entire device and offset quantum-well gain layers are included at the laser gain and SOA sections.

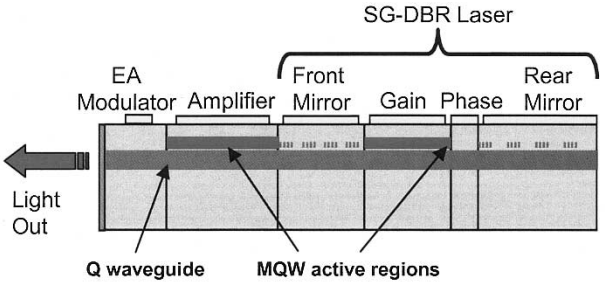

Fig. 8. Single-chip widely-tunable transmitter schematic showing a SGDBR laser integrated with an SOA and EAM.

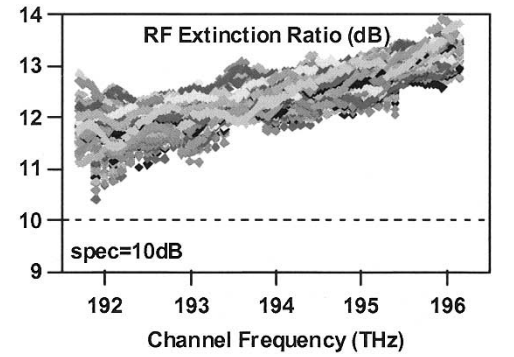

(a)

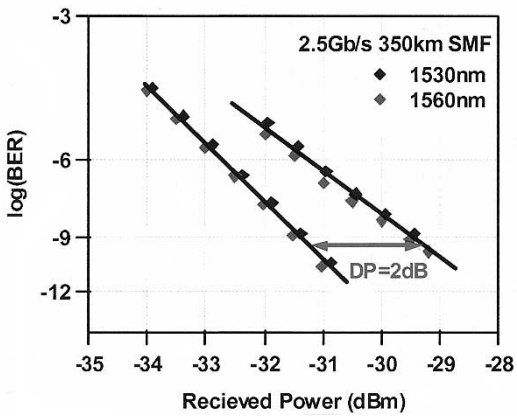

(b)

Fig. 9. (a) RF extinction ratio for 100 superimposed SGDBR/EAM transmitters across the *C*-band. (b) Bit-error-rate results after transmission through 350 km of standard fiber at 2.5 Gb/s.

Fig. 8 shows a schematic cross section of an InP-based transmitter chip [28] as included in the photos of Fig. 6. The modulator bias is varied across the 40 nm tuning range to enable efficient modulation and good extinction across this entire range.

Fig. 9(a) shows superimposed rf-extinction ratio versus wavelength characteristics for 100 transmitter chips across the *C*-band, and Fig. 9(b) shows the bit-error rate after transmission through 350 km of standard single-mode fiber for two different wavelengths. The data is applied directly to the EAM of the chip. The average modulated output power is about 3 dBm in this case. Error-free operation was observed.

The transmitter illustrated in Figs. 6 and 8 and characterized in Fig. 9 provides good results at 2.5 Gb/s for distances up to 350 km. However, for longer distances and/or higher bit rates, some sort of chirp control is necessary. Thus, work at both Agility [6], [29] and UCSB [30] has explored replacing the EAM with a Mach-Zehnder modulator (MZM) as shown in Fig. 10. Such modulators have been used widely for long-haul applications, and they allow negative chirp with only one drive signal, although dual drive of both arms of the MZM are necessary for truly programmable chirp. In the past, researchers have had difficulties in integrating such MZM's directly with lasers because of reflections. However, the UCSB-Agility effort appears to have solved these difficulties. By monolithically integrating the MZM a much smaller footprint and low power dissipation is possible as compared to hybrid packaged or fiber-coupled devices. In addition, the chirp can be tailored for each channel across the wavelength band by adjusting the biases to the two legs of the MZM. Chirp values from $+1$ to -1 are readily available. Error free transmission over 80 km of standard fiber was demonstrated for all channels at 10 Gb/s using a negative chirp configuration.

VI. Reliability of the SGDBR Laser

Fig. 11 summarizes some of the reliability data taken on the 10 mW cw product by Agility [31]. Both the integrated EAM transmitter and the 10 mW cw version have undergone complete Telcordia qualification. Because of the InP single-chip architecture, these PICs can be qualified in much the same way as simple laser chips. Such is not the case with other types of widely-tunable transmitters in which separated optical parts are involved in some sort of hybrid package.

A quantitative model of failure rates was developed for each section of the device by fully characterizing failure modes and determining failure mode accelerants. The activation energy, $E_a = 0.5$ eV was derived assuming an aging rate proportional to $\exp[E_a/kT]$. The current acceleration exponent, $n = 1.5$ was derived assuming the aging rate was also proportional to J^n, where J is the applied current density to the section in question. Mirror drift failure was set to be when the operating point moved half way from the center of a single-mode region toward a mode-hop boundary. For the SGDBRs in question this was equivalent to ± 100 pm of allowable open-loop wavelength drift of the mode boundaries. (Of course, with a wavelength locker in operation, the lasing mode wavelength only drifts as much as it does—typically <1 pm over life.) The aging criteria for the gain and amplifier sections are as for other semiconductor lasers. The same approximate activation energies and current acceleration factors were observed for all sections.

The data indicate that no updating of mirror currents is necessary for a FIT rate of <20 at 15 years. This includes reasonable margins for all device parameters. However, a mirror look-up table updating algorithm has also been developed that both monitors the mirror drift for setting possible alarms as well as updating the table. This mirror-control algorithm improves the FIT rate to <3 at 15 years. The lifetime distribution taken from 200 parts using accelerated aging procedures shows a classical log-normal relationship with a mean lifetime of 186 years for room temperature, but with maximum channel currents assumed. In a normal WDM system populated with such devices, the channel currents would be distributed over lower values for the various channels, so Fig. 11 should be taken as a worst case

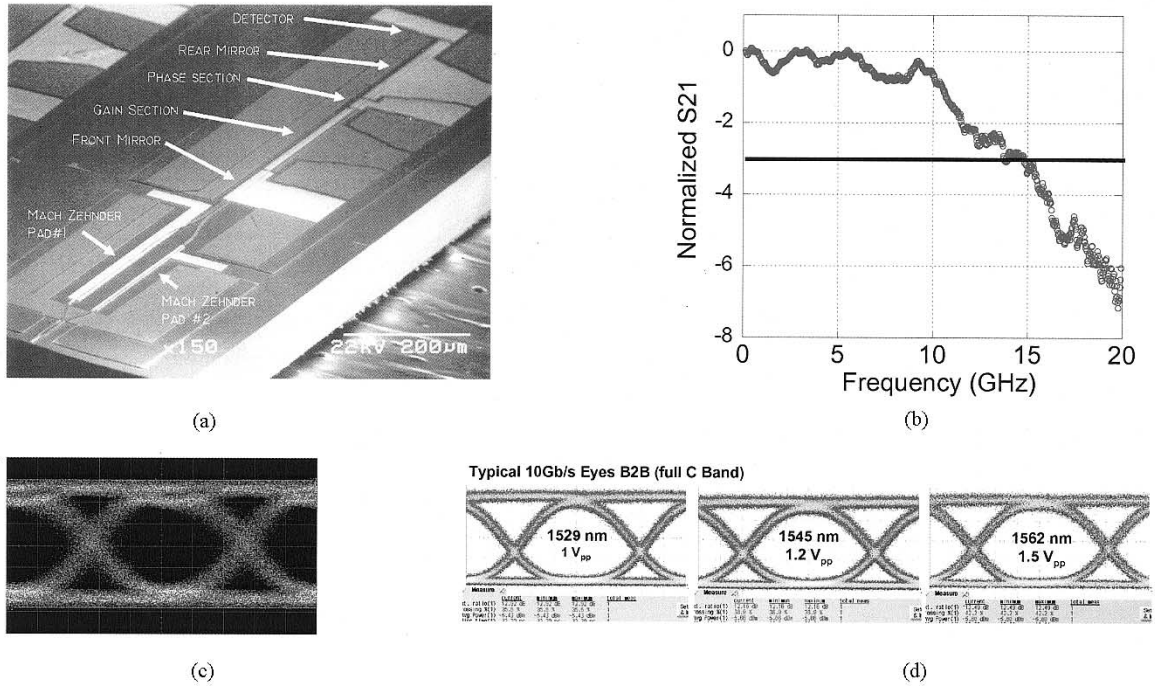

Fig. 10. (a) SEM photo of UCSB's SGDBR integrated with a Mach-Zehender modulator, (b) small-signal bandwidth, (c) unfiltered eye, and (d) filtered eye-diagrams at 10 Gb/s for three wavelengths across the band for Agility device.

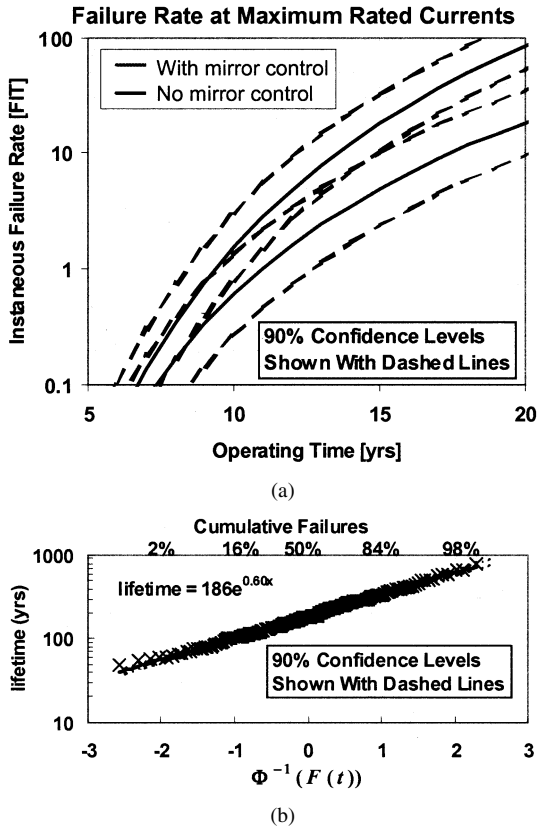

Fig. 11. (a) FIT rate versus time, assuming both original mirror biases as well as with bias updating-mirror control. (b) Lifetime distribution of 200 parts tested. Maximum channel currents assumed. Mean lifetime of 186 years shown.

result that would not occur over any distribution of components in a typical system. Taking a distribution of WDM channels into account, the "no mirror control" FIT rate is estimated to be about 2 @ 15 years.

This relatively low wavelength drift for the SGDBR has been ascribed to the relatively small percentage of grating that fills the sampled-grating mirrors. About 90% of the mirror area is free from gratings in a typical design. Studies have shown that this results in much higher material quality within the mirrors [31]. Lack of gratings in most areas permits very high quality regrowth of the InP cladding following grating formation. Not only is the surface more planar and free from defects, it can be composed of InP rather than InGaAsP quaternary waveguide material in the large regions between the grating bursts. Thus, while standard DBR lasers, which contain gratings throughout the mirror tuning sections, continue to have wavelength drift problems, the SGDBR has emerged as being surprisingly stable.

VII. Control of Widely-Tunable Lasers

The control of multi-element tunable lasers, such as those illustrated in Fig. 5, has been a roadblock to their general acceptance for some time. Most system engineers are accustomed to incorporating a two-terminal device, such as a DFB laser, in their optical transmitters. Of course, even for the DFB the device temperature is used to fine tune and lock the wavelength in WDM systems. For the widely-tunable devices of Fig. 5, it seems apparent that we must simultaneously control some additional parameters, although in some cases we may only need to dynamically control the same number as in the DFB to lock the amplitude and wavelength at a given channel. However, there is always a need for a "look-up table" to give the specific set of currents or voltages for each channel to the several sections, and this indeed, does add a complication for the user. To gain

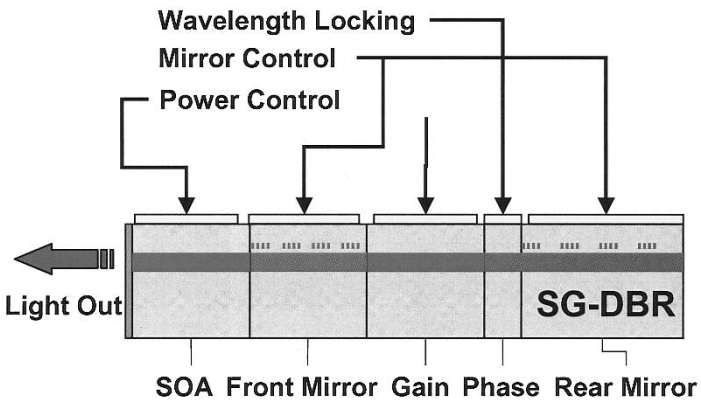

Fig. 12. SGDBR/SOA with connections for control circuit.

more wide-spread acceptance, suppliers of the multiple-section lasers in recent years have provided automatic control systems within the laser module so that the user doesn't have to deal with the control problem. The wavelength and amplitude are set via a digital command through a common interface. Nevertheless, users are justifiably concerned with the reliability and stability of such systems. So they remain of great interest.

The control system must be capable of two basic functions: 1) staying accurately on the desired wavelength channel and 2) reliably finding a new desired channel when a channel change is requested at some later time, and this time could be near the end of life. To accurately stay on a desired wavelength channel most lasers require a separate wavelength locker. If the wavelength channel plan is relatively coarse, perhaps >100 GHz, this locker may not be necessary. For example, given the low wavelength drift of the SGDBR outlined above, this locker may not be necessary for even 100 GHz channel spacing if a modest FIT rate is tolerable. But, more generally a locker is required. It usually contains an etalon with a free-spectral range roughly equal to the channel spacing, so that it can provide a feedback signal to capture and lock the wavelength within about one-third of a channel spacing on either side of some ITU frequency.

Switching to a new channel after some time is generally a more difficult problem. The immediate question is, will the original look-up table from factory calibration be good enough, or will aging have changed the values? To be able to use the original look-up table, the settings must get us to the correct channel within the capture range of the locker. For embodiments where tuning requires mechanical motion or significant swings in temperature, hysteresis and charging of MEMs elements tend to shift the look-up table. In some DBR structures, changes in carrier lifetime also may result in a shift in wavelength that exceeds the locker capture range. Possible solutions to these problems involve either some sort of global wavelength monitor, a channel counting algorithm, or some means of updating the look-up tables over life. All of these approaches have been demonstrated, but all require a more complex control system.

Fig. 12 illustrates the control signals necessary to operate the SGDBR/SOA. An electronic circuit supplies control currents in response to amplitude and wavelength errors derived from the locker. The temperature and the current to the gain section are held constant at factory-set values, so they are not part of the control system. All other currents are contained in a look-up table for each channel. The locker signals are converted to error currents for that are added to the SOA and phase sections. The SOA is used to lock the amplitude and the phase section is used to lock the wavelength. In normal operation no corrections are supplied to the mirrors—this is called the "no mirror control" case referred to in Fig. 11. In this mode of operation then, the actual feedback control system is about the same as for the DFB, with the amplitude correction being added to the SOA instead of the DFB gain section and the wavelength correction being added to the phase section instead of the thermoelectric cooler of the DFB. Of course, there is a look-up table to set different initial values for each channel in the SGDBR case, but this involves no dynamic control, just set points.

It may also be seen that the use of an external SOA for amplitude control is desirable in a tunable laser relative to adjusting the gain current in the cavity. This is because the wavelength would also change in response to changing the gain current. In fact, this is one of the primary limitations on wavelength stability in widely-tunable laser embodiments that do not have the external SOA to level the amplitude as the device ages.

For "mirror control" the mirror currents are slowly dithered about their set points and the voltage on the gain section is monitored. Because the wavelength and amplitude locking circuits are operating, there is no change in external optical power or wavelength observed. Second order changes in cavity loss, caused by changing the mirror currents, are also removed in this process. The dithering of the reflectivity peaks of the mirrors cause the gain voltage to change slightly because it monitors the quasi-Fermi level separation in the gain region, and this is proportional to the cavity loss change. Thus, a local minimum in the gain voltage is observed when the mirror peaks are properly aligned with the mode wavelength, where the cavity loss is at a local minimum. The mode, of course, is set by the locker/phase-section feedback circuit to be at the proper ITU grid wavelength. So, it can be seen that this "mirror control" algorithm requires no additional optical elements or electrical connections. Again, this mirror control mode is probably not necessary for reliable device operation according to Fig. 11; however, monitoring of the mirror peaks relative to the cavity mode gives one assurance that the device is operating properly.

If the mirror currents must be corrected, then it may be assumed that the currents required to hit other channels must also change. This is the second aspect of control mentioned

TABLE I
CONTROL PARAMETERS FOR TUNABLE LASERS

Laser	Coarse Wavelength	Fine Wavelength	Amplitude	VOA
DFB Array/SOA	$V_{array}(j)$	T	$I_{gain}(j)$	ΔI_{SOA}
DFB/MEMs	V_{m1}, $V_{m2}(j)$	T	$I_{gain}(j)$	Vm1, $V_{m2}(j)$
SGDBR/SOA	I_{m1}, I_{m2}	I_ϕ	I_{SOA}	ΔI_{SOA}
Ext Cavity/ grating	$V_{m\theta}$	V_{mL} or I_ϕ	I_{gain}	$V_{mshutter}$
Ext. Cavity/ etalons	T_{et1}, T_{et2}	V_{mL} or I_ϕ	I_{gain}	---
VCSEL/MEMs	V_{m1}	V_{m1}	I_{gain}	---

above—finding a new channel. In the SGDBR case with mirror control the table can be updated dynamically without ever leaving the original channel. This is because the same reduction in carrier lifetime that requires a current increase to maintain a given carrier density and thus index of refraction, is also experienced by all the other channels. Most importantly, it has been verified that this carrier lifetime decrease is due to an increase in nonradiative recombination, and it is well known that this has a linear relationship to carrier density. Since carrier density is predominately determined by the radiative recombination rate, which depends upon the square of the carrier density, we can assume that the shift in the entire look-up table will be linear in the square root of current. Fortunately, extensive measurements have shown that this is indeed the case experimentally [31], [32], so updating the table is a valid approach in this case.

Table I summarizes the parameters that must be adjusted to enable the amplitude and wavelength of the various types of tunable lasers illustrated in Fig. 5 to be set. It also indicates the parameters for variable-optical-attenuator (VOA) operation. This function is desirable both to allow the user to adjust the amplitude as well as to blank the output during tuning between channels. As can be seen most of the widely-tunable lasers being considered require several parameters to be set, and in most cases, most of these must be controlled. In the VCSEL/MEMs case there are fewer parameters, but this is an example where changing channels requires some sort of global wavelength monitor or channel counting scheme, because one clearly can not depend upon the look-up table for channel selection, especially after some aging with the MEMs mirror. The case is similar in the other mechanically tuned embodiments.

VIII. CONCLUSION

As presented in the tutorial on tunable semiconductor lasers at OFC'03 we have outlined why tunable lasers might be beneficial, discussed basic tuning mechanisms involved in most tunable lasers, given some examples of tunable lasers that have been commercialized, discussed reliability issues, and outlined control techniques. A summary of performance data for the SGDBR type of laser and the monolithically integrated SGDBR with both electroabsorption and Mach-Zehnder modulators was given. It was argued that tunable lasers can reduce operational costs, that full-band tunability is desirable for many applications, that monolithic integration offers the most potential for reducing size, weight, power and cost, and that sufficient reliability for system insertion has been demonstrated, at least in the SGDBR case.

REFERENCES

[1] L. Coldren, "Monolithic tunable diode lasers," *IEEE J. Select. Topics Quantum Electron.*, vol. 6, p. 988, Nov./Dec. 2000.
[2] R.-C. Yu *et al.*, presented at the Proc. APOC'03, Wuhan, China, Sept. 3, 2003.
[3] G. Fish and K. Affolter, "Tunable lasers and their impact on optical networks," presented at the Communications Design Conf., San Jose, CA, Aug. 2002.
[4] D. J. Blumenthal, B. E. Olsson, G. Rossi, T. Dimmick, L. Rau, M. L. Ma'anovic', O. A. Lavrova, R. Doshi, O. Jerphagnon, J. E. Bowers, V. Kaman, L. A. Coldren, and J. Barton, "All-Optical label swapping networks and technologies," *IEEE J. Lightwave Technol., Special Issue Optical Networks*, vol. 18, pp. 2058–2075, Dec. 2000.
[5] M. L. Mašanović, V. Lal, J. S. Barton, E. J. Skogen, L. A. Coldren, and D. J. Blumenthal, "Monolithically integrated Mach-Zehnder interferometer wavelength converter and widely-tunable laser in InP," *IEEE Photon. Technol. Lett.*, vol. 15, pp. 1115–1117, Aug. 2003.
[6] L. A. Coldren, "Widely-tunable chip-scale transmitters and wavelength converters," in *Integrated Photonics Research Tech. Dig.*, Washington, DC, June 2003, Paper IMB-1, pp. 6–8.
[7] A. Carena, M. D. Vaughn, R. Gaudino, M. Shell, and D. J. Blumenthal, "OPERA: An optical packet experimental routing architecture with label swapping capability," *IEEE J. Lightwave Technol., Special Issue Photonic Packet Switching Technologies, Techniques, and Systems*, vol. 16, pp. 2135–2145, Dec. 1998.
[8] M. Duelk, J. Gripp, J. Simsarian, A. Bhardwaj, P. Bernasconi, M. Zirngibl, and O. Laznicka, "Fast packet routing in a 2.5 Tb/s optical switch fabric with 40 Gb/d duobinary signal at 0.8 b/s/Hz spectral efficiency," presented at the OFC 2003, 2003, postdeadline paper PD8-1.
[9] L. A. Coldren and S. W. Corzine, *Diode Lasers and Photonic Integrated Circuits*. New York: Wiley, 1995.
[10] M. C. Amann and J. Buus, *Tunable Laser Diodes*. London: Artech, 1998.
[11] N. Natakeyama, K. Naniwae, K. Kudo, N. Suzuki, S. Sudo, S. Ae, Y. Muroya, K. Yashiki, S. Satoh, T. Morimoto, K. Mori, and T. Sasaki, "Wavelength -Selectable microarray light sources for S-, C-, and L-band WDM systems," *IEEE Photon. Technol. Lett.*, vol. 15, pp. 903–905, 2003.
[12] M. Bouda, M. Matsuda, K. Morito, S. Hara, T. Watanabe, T. Fujii, and Y. Kotaki, "Compact high-power wavelength selectable lasers for WDM applications," in *Proc. OFC 2000*, vol. 1, Mar. 2000, pp. 178–180.

[13] J. Heanue, E. Vail, M. Sherback, and B. Pezeshki, "Widely tunable laser module using DFB array and MEM's selection with iternal wavelength locker," in *Proc. OFC 2003*, vol. 1, 2003, pp. 82–83.
[14] D. Anthon, J. D. Brerger, J. Drake, S. Dutta, A. Fennema, J. D. Grade, S. Hrinya, F. Ilkov, H. Jerman, and D. King, "External cavity diode lasers tuned with silicon MEMS," in *Proc. OFC 2003*, 2002, pp. 97–98.
[15] T. Day. "External-cavity tunable diode lasers for network deployment". presented at Proc. OFC 2001. [Online]. Available: http://www.newfocus.com/Online_Catalog/Literature/Tunable2.pdf
[16] *Intel Work* [Online]. Available: http://www.commsdesign.com/story/OEG20 030 110S0053
[17] K. J. Knopp, D. Vakhshoori, P. D. Wang, M. Azimi, M. Jiang, P. Chen, Y. Matsui, K. McCallion, A. Baliga, F. Sakhitab, M. Letsch, B. Johnson, R. Huang, A. Jean, B. DeLargy, C. Pinzone, F. Fan, J. Liu, C. Lu, J. Zhou, H. Zhu, and R. Gurjar, "High power MEMs-tunable vertical-cavity surface-emitting lasers," in *Proc. Advanced Semiconductor Lasers, Dig. LEOS Summer Topical Meet.*, Copper Mountain, CO, July–Aug. 30–1, 2001, pp. 31–32.
[18] C. J. Chang-Hasnain, "Tunable VCSEL's," *IEEE J. Select. Topics Quantum Electron.*, vol. 6, pp. 978–987, Nov.–Dec. 2000.
[19] T. L. Koch, U. Koren, and B. I. Miller, "High-performance tunable 1.55 mm InGaAs/InGaAsP multiple-quantum-well distributed-bragg-reflector lasers," *Appl. Phys. Lett.*, vol. 53, pp. 1036–1038, 1988.
[20] J. E. Johnson, L. J. Ketelsen, D. A. Ackerman, L. Zhang, M. S. Hybertsen, K. G. Glogovsky, C. W. Lentz, W. A. Asous, C. L. Reynolds, J. M. Geary, K. K. Kamath, C. W. Ebert, M. Park, G. J. Przybylek, R. E. Leibenguth, S. L. Broutin, and J. W. Stayt Jr, "Fully stabilized electroabsorption-modulated tunable DBR laser transmitter for long-haul optical communications," *IEEE J. Select. Topics Quantum Electron.*, vol. 7, pp. 168–177, Mar.–Apr. 2001.
[21] H. Debregeas-Sillard, A. Vuong, F. Delorme, J. David, V. Allard, A. Bodere, O. LeGouezigou, F. Gaborit, J. Rotte, M. Goix, V. Voiroit, and J. Jacquet, "DBR module with 20 mW constant coupled output power, over 16 nm (40×50 GHz spaced channels)," *Photon. Technol. Lett.*, vol. 13, no. 1, pp. 4–6, Jan. 2001.
[22] M. Oberg, S. Nilsson, K. Streubel, J. Wallin, L. Backborn, and T. Klinga, "74 nm wavelength tuning range of an InGaAsP/InP vertical grating assisted codirectional coupler laser with rear sampled grating reflector," *IEEE Photon. Tech. Lett.*, vol. 5, pp. 735–738, 1993.
[23] B. Broberg, P. J. Rigole, S. Nilsson, L. Andersson, and M. Renlund, "Widely tunable semiconductor lasers," in *Proc. OFC/IOOC '99*, vol. 2, Feb. 1999, pp. 137–139.
[24] V. Jayaraman, A. Mathur, L. A. Coldren, and P. D. Dapkus, "Theory, design, and performance of extended tuning range in sampled grating DBR lasers," *IEEE J. Quantum Electron.*, vol. 29, pp. 1824–1834, June 1993.
[25] B. Mason, J. Barton, G. A. Fish, L. A. Coldren, and S. P. Denbaars, "Design of sampled grating DBR lasers with integrated semiconductor optical amplifiers," *IEEE Photon. Technol. Lett.*, vol. 12, pp. 762–764, 2000.
[26] Y. Tohmori, Y. Yoshikuni, H. Ishii, F. Kano, T. Tamamura, Y. Kondo, and M. Yamamoto, "Broadrange wavelength-tunable superstructure grating 9SSG) DBR lasers," *IEEE J. Quantum Electron.*, vol. 29, pp. 1817–1823, 1993.
[27] C. Coldren *et al.*, "Workshop on tunable lasers," presented at the OFC'03 Proc., Atlanta, GA, Mar. 2003.
[28] Y. A. Akulova, G. A. Fish, P.-C. Koh, C. L. Schow, P. Kozodoy, A. P. Dahl, S. Nakagawa, M. C. Larson, M. P. Mack, T. A. Strand, C. W. Coldren, E. Hegblom, S. K. Penniman, T. Wipiejewski, and L. A. Coldren, "Widely tunable electroabsorption-modulated sampled-grating DBR laser transmitter," *IEEE J. Select. Topics Quantum Electron.*, vol. 8, no. 6, pp. 1349–1357, 2002.
[29] T. Wipiejewski, Y. Akulova, G. Fish, P. Koh, C. Show, P. Kozodoy, A. Dahl, M. Larson, M. Mack, T. Strand, C. Coldren, E. Hegblom, S. Penniman, T. Liljeberg, and L. Coldren, "Performance and reliability of widely-tunable laser diodes," in *Proc. Electronic Components and Technology Conf.*, New Orleans, LA, May 2003, pp. 789–795.
[30] J. S. Barton, E. J. Skogen, M. L. Masanovic, S. P. DenBaars, and L. A. Coldren, "Widely-tunable high-speed transmitters using integrated SGDBR's and Mach-Zehnder modulators," *IEEE J. Select. Topics Quantum Electron.*, vol. 9, 2003.
[31] C. Coldren, T. Strand, E. Hegblom, Y. Akulova, G. Fish, M. Larson, and L. Coldren, "Reliability of widely-tunable SGDBR lasers suitable for deployment in agile networks," in *OFC Tech. Dig.*, Atlanta, GA, Mar. 2003, Paper MF60.
[32] D. A. Ackerman, J. E. Johnson, G. Chu, S. Nee, Z. Liming, E. J. Dean, and L. J.-P. Ketelsen, "Assessment and modeling of aging in electro-absorption distributed bragg reflector lasers," *IEEE J. Quantum Electron.*, vol. 37, pp. 1382–1387, Nov. 2001.

Larry A. Coldren (S'67–M'72–SM'77–F'82) received the Ph.D.d egree in electrical engineering from Stanford University, Stanford, CA, in 1972.

He is the Fred Kavli Chair of Optoelectronics and Sensors at the University of California, Santa Barbara (UCSB). He is also Chairman and Chief Technology Officer of Agility Communications Inc., Santa Barbara, a company he cofounded in 1998 to develop widely tunable transmitters for wavelength-division multiplexed networks. After 13 years in the research area at Bell Laboratories, he joined UCSB in 1984, where he now holds appointments in Materials and Electrical & Computer Engineering and is Director of the Optoelectronics Technology Center. At UCSB, his efforts have included work on guided-wave and vertical-cavity modulators and lasers as well as the underlying materials growth and fabrication technology. His current work includes the integration of these devices to create novel optical transmitters, receivers, and wavelength converters for optical networking and interonnection. He has authored or coauthored over 500 papers, 5 book chapters, 1 textbook, and has been issued 36 patents.

Prof. Coldren is a Fellow of the Optical Society of America and the Institute of Electrical Engineers (U.K.).

G. A. Fish, photograph and biography not available at the time of publication.

Y. Akulova, photograph and biography not available at the time of publication.

J. S. Barton, photograph and biography not available at the time of publication.

L. Johansson, photograph and biography not available at the time of publication.

C. W. Coldren (S'97–M'00), photograph and biography not available at the time of publication.

Scalable and Reliable Photonic Integrated Circuits for Scalable and Reliable WDM Networks

(Plenary paper)

Larry A. Coldren

University of California and Agility Communications, Inc.

Santa Barbara, CA 93106

Tel: (805) 893-4486; Fax: (805) 893-4500; email: coldren@ece.ucsb.edu

Abstract

Photonic ICs that function as reliable single-chip widely-tunable transmitters have been developed on a simple InP-based platform technology. This same platform has been shown to be scalable to more than a dozen optical elements for more complex functionalities such as full-band wavelength converters. Much higher levels of integration are anticipated.

Summary

The allure of monolithically integrating many photonic components to form high-performance photonic integrated circuits (PICs) has been with us for many years. Such devices, as their electronic-IC counterparts, should provide improved performance and reliability, while having lower power, size, weight, and cost than their discrete-component embodiments. Moreover, the integration technology should be scalable so that more and more photonic components can be integrated as the technology matures to provide further improvements in these key parameters. This is a nice vision, but until recently most efforts to create such PICs have largely fallen short of the goal. In this paper we shall summarize recent progress in developing a robust InP-based platform technology that is capable of providing scalable and reliable PICs, which in some forms are now ready for wide-scale deployment in WDM networks.

Figure 1 gives a schematic and an SEM photo of an integrated PIC transmitter, which includes a widely-tunable laser, a back-side monitoring detector, a semiconductor optical amplifier (SOA), and an electroabsorption modulator (EAM)[1]. The integration platform includes only one regrowth step to form the gratings and define the active and passive regions. The entire transmistter is fabricated with the same layer structure and the same fabrication process as the laser alone.

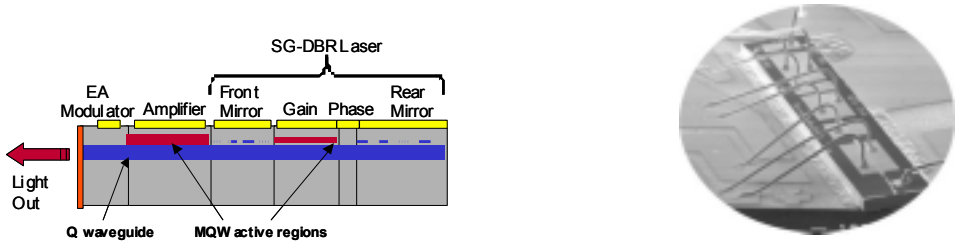

Figure 1. Schematic and SEM of single-chip transmitter.

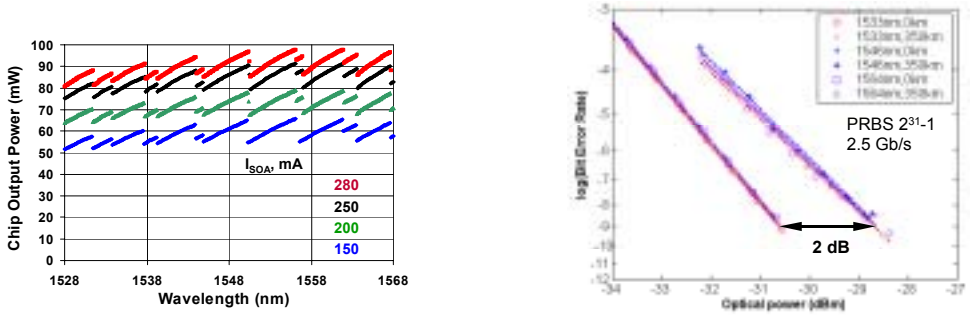

Figure 2. Unleveled cw chip power vs. wavelength (left) and BER of the packaged transmitter for several wavelengths (right) across the C-band after transmission over 350 km on standard fiber.

Figure 2 shows that relatively high powers are available from these chips and that the packaged chips can give very competitive transmitter performance.

These devices have undergone extensive reliability testing and have shown very stable operation over life[2]. In fact, the open-loop wavelength is surprisingly stable on these SGDBR lasers as compared to previous reports on DBR lasers[3], and the results compare favorably to the stability of DFB lasers. The explanation for this seems to lie in the fact that the SGDBR mirrors only contain a small fraction of grating, and the space between the grating bursts, which provides an InP-on-InP regrowth surface, actually determines the mirror peak position. Thus, mode hops never occur within the lifetime of the gain section, which extends to several hundred years for a 20% roll off in power as determined by rigorous Telcordia standards. Moreover, the dual grating SGDBR laser design has a much larger design window than simple DBRs. Mirrors can be misaligned by more than 50% without degrading the side-mode-suppression ratio (SMSR) to less than 40dB.

More recently, state-of-the-art Mach-Zehnder modulators have been successfully integrated on the same chip as the SGDBR, detector, and SOA[4,5]. Figure 3 illustrates a schematic and SEM of the chip as well as transmission results at 10Gb/s. This represents a still higher level of integration, because the chip now includes MMI power splitters and combiners and additional phase shifters for the ultimate in chirp control. The effective chirp parameter has been shown to be programmable from +1 to –1. In Fig. 3, a chirp parameter of approximately –0.7 was set to provide error-free transmission over 100km of standard fiber across the entire C-band.

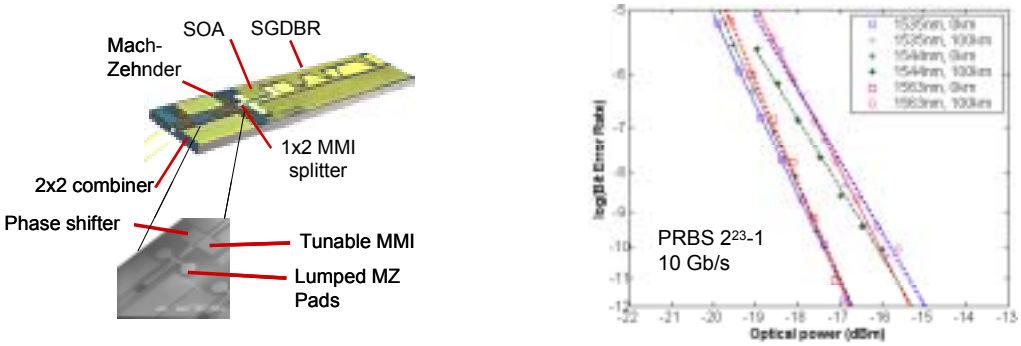

Figure 3. Schematic, SEM blowup, and transmission results with integrated transmitter using an integrated Mach-Zehnder modulator.

Most recently, the integration platform has been extended to include additional functionalities as well as to make arrays of devices. All-optical wavelength converters, incorporating SOAs modulated by optical data on preamplified inputs[6], as well as photocurrent-driven wavelength converters that used SOA-PIN input stages directly coupled to either the SGDBR gain section or the integrated external modulator[7] have been demonstrated with error free operation over a wide bandwidth of input and output wavelengths. Yields for these complex devices appear to be similar to the SGDBR itself, and these have been reported to exceed DFB yields.

Conclusions

A PIC integration platform on InP has been demonstrated to provide high-performance, high-reliability devices with significant numbers of elements on a single chip. The design rules require that all other devices must be integrable with the same layer structure and processing steps as required for the widely-tunable SGDBR laser alone. Future plans call for significant increases in the level of integration from this platform.

References:

[1] Y. A. Akulova, G. A. Fish, et al., "Widely tunable electroabsorption-modulated sampled-grating DBR laser transmitter", *IEEE Journal of Selected Topics in Quantum Electron*., v.8, no. 6 , pp.1349-1357, 2002.
[2] C. Coldren, T. Strand, E. Hegblom, Y. Akulova, G. Fish, M. Larson, and L. Coldren, *OFC Tech Dig*., pap. MF60, Atlanta, Mar. 2003.
[3] D. A. Ackerman, J.E. Johnson, George Chu, Sung Nee, Zhang Liming, E.J. Dean, L.J.-P. Ketelsen, "Assessment and modelling of aging in electro-absorption distributed Bragg reflector lasers," *IEEE J Quantum Electron*., **37**, pp1382-1387, 2001.
[4] J. S. Barton, E.J. Skogen, M.L. Masanovic, S. P. DenBaars, and L. A. Coldren, "Widely-tunable high-speed transmitters using integrated SGDBRs and Mach-Zehnder modulators," *JSTQE*, **9,** Semi. Lasers issue, 2003.
[5] L.A.Coldren, "Integrated tunable transmitters for WDM networks," *Proc. ECOC-IOOC'03*, Rimini, pp. 878-881, Sept, 2003.
[6] M. L. Mašanović, V.Lal, J.S. Barton, E.J. Skogen, L.A. Coldren, D.J. Blumenthal,, "Monolithically Integrated Mach-Zehnder Interferometer Wavelength Converter and Widely-Tunable Laser in InP", *IEEE Photonics Technology Letters*, August 2003.
[7] J.M. Hutchinson, J.A. Henness, L.A. Johansson, et al, "2.5 Gb/s wavelength conversion using monolithically-integrated photodetector and directly modulated widely-tunable SGDBR laser," *Proc. LEOS'03*, Tucson, Oct. 2003.

Sampled-grating DBR laser integrated with SOA and tandem electroabsorption modulator for chirp-control

L.A. Johansson, Y.A. Akulova, G.A. Fish
and L.A. Coldren

Chirp-controlled optical modulation is demonstrated using a voltage division scheme applied to a long-section phase modulator to compensate for the positive chirp of an electroabsorption modulator arranged in a tandem configuration. Both modulators are integrated with a semiconductor optical amplifier (SOA) and a sampled-grating distributed Bragg reflector (DBR) laser. The effective chirp factor can be controlled from +1 to −0.86 with less than 2 dB penalty in extinction ratio and insertion loss.

Introduction: Widely tunable lasers integrated with electroabsorption modulators generally use a Franz-Keldysh modulator for wide spectral bandwidth [1]. The positive chirp of these modulators is a limiting factor for data transmission over long spans of fibre. Negative chirp and wide spectral bandwidth can be offered by integration of a widely tunable laser with a Mach-Zehnder modulator [2] at the cost of more complex modulator design and increased passive loss of the modulator. An alternative approach to generate negative chirp is using two EA modulators in a tandem configuration, one biased for amplitude modulation, the other biased for phase modulation using an inverted driver signal, compensating for the residual phase modulation of the amplitude modulator [3]. This approach is limited by the voltage swing available at the phase modulator, determined on the high voltage side by the diode threshold voltage, where carrier injection is causing distortion, and limited on the low voltage side by the onset of absorption that ultimately makes the insertion loss prohibitive and deteriorates the extinction ratio. One possibility to enhance the available performance of this approach is to use different bandgap EA modulators, possible to achieve using quantum-well intermixing techniques [4]. A second possibility that applies to Franz-Keldysh modulators is to use a simple voltage division scheme, which is described in this Letter.

Device design: Fig. 1 shows a schematic diagram of the device used in this work together with the voltage division scheme used. The electroabsorption modulator is split in two parts arranged in a tandem configuration. The device is mounted onto an aluminium nitride RF carrier, with integrated thin-film resistors. The amplitude modulator is terminated in parallel to 50 Ω in series with a capacitor. In contrast, the phase modulator is terminated in parallel by a lower value resistor and in series by a second resistor, such that $R_1 + R_2 = 50\ \Omega$. The resulting voltage division factor, n, is given by $n = 50\ \Omega/R_1$. To compensate for the lower modulation voltage, the phase modulator is made n times longer than the amplitude modulator. To a first-order estimate, the *RC*-limited bandwidth of the modulators remains the same. The main advantage of the described voltage division scheme is that while the modulation voltage is now scaled down by a factor of n, the threshold voltage stays constant, increasing the available phase swing while keeping amplitude modulation in the phase modulator low.

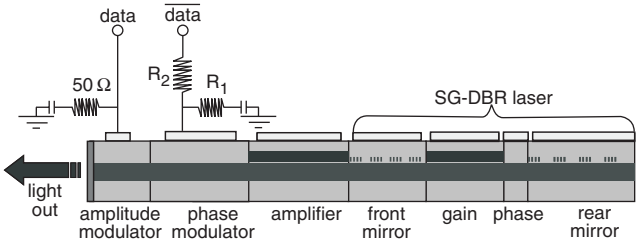

Fig. 1 *Schematic diagram of tandem EAM modulator, integrated with SOA and sampled-grating DBR laser; simple schematic of voltage division scheme also shown*

Two devices are investigated, the first having a 200 μm amplitude modulator and an 800 μm phase modulator, with a voltage division factor of $n = 4$. The second device has equal length sections of 120 μm, and is used for verification of the benefits of the principle. The sampled-grating DBR lasers are similar to the one described in [2], with more than 10 mW output power, lower than 2 MHz linewidth, and more than 40 dB side-mode suppression ratio, achieved over more than 40 nm wavelength tuning range.

Experimental results: The amplitude modulator is modulated at 2.5 Gbit/s datastream while the phase modulator is complementary modulated by the inverted signal. By varying the attenuation/amplification of the signal applied to the phase modulator, the resulting chirp of the device can be controlled. The time-resolved chirp characteristics of the modulated optical signal is measured using an Advantest Q7606B optical chirp form test set and an Agilent 86100A oscilloscope. The effective chirp factor, α_{eff}, is then derived from the time-resolved chirp data. Previously, using the amplitude modulator only, the effective chirp parameter has been shown to correlate well to the fibre dispersion penalty for this type of device [5].

Fig. 2 shows the measured chirp forms for the device when voltage division of $n = 4$ was used. The phase modulator was biased at 0 V and the amplitude modulator at −2.6 V. The upper plot shows the chirp characteristics of the amplitude modulator alone, corresponding to an α_{eff} of 0.97. Applying a modulation signal to the phase modulator of equal amplitude as to the amplitude modulator, results in the characteristics shown by the centre plot, corresponding to α_{eff} of 0.03. The remaining frequency chirping, particularly apparent at the falling edge, is a result of different impulse response between the phase and amplitude modulator. The different impulse response can be attributed in part to the inductance of the bondwire used to connect the modulators to the RF lines of the carrier. A more careful RF design should further decrease the envelope of the frequency chirp. The lower plot in Fig. 2 shows α_{eff} of −0.86 for a phase modulation signal amplified by 3 dB relative to that of the amplitude modulator.

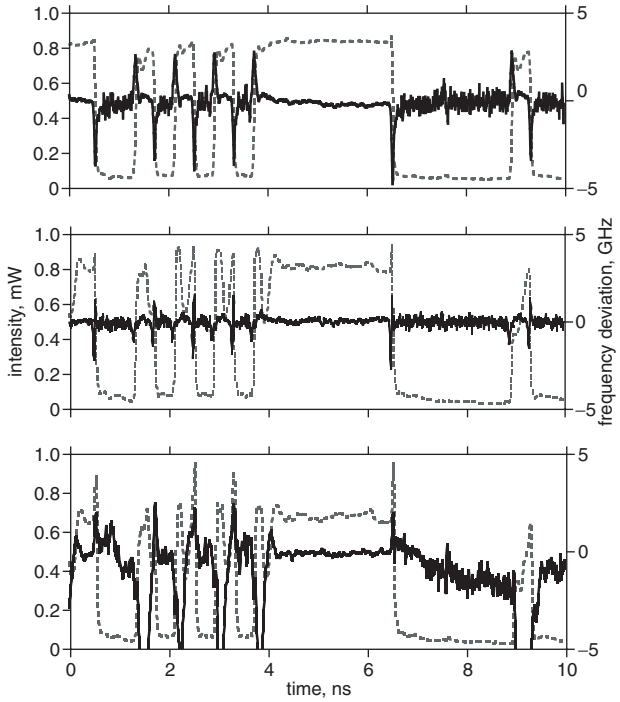

Fig. 2 *Measured output amplitude (dotted line) and time-resolved frequency chirping (solid line) of tandem EAM configuration*
Resulting effective chirp factors 0.97, 0.03, −0.86, respectively, top to bottom

Fig. 3 shows the extinction and excess insertion loss compared to amplitude modulation only against achieved effective chirp factor for a device using voltage division and a control device with equal length modulators. Significant penalties are shown for the control device at lower chirp values, as a result of counteracting amplitude modulation in the phase modulator. Using voltage division, α_{eff} down to −0.86 is observed with <2 dB excess insertion loss and <2 dB degradation of extinction ratio. For even lower values of achieved effective chirp, further degradation is observed, partly due to too high applied voltage in the phase modulator. This can be traded-off with a slightly degraded

insertion loss and extinction by lowering the bias point of the phase modulator.

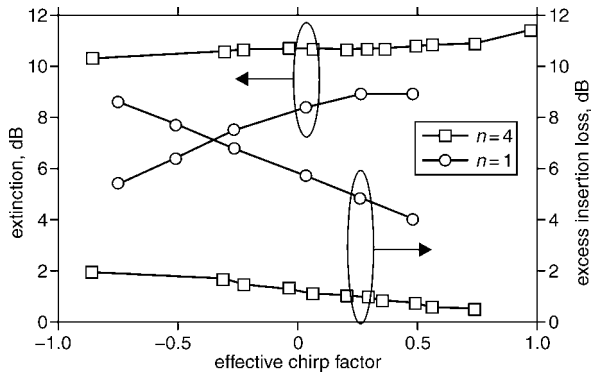

Fig. 3 *Extinction ratio and resulting penalty in terms of insertion loss, compared to amplitude modulation only, against measured large-signal chirp factor for $n = 4$ and $n = 1$*

The control device achieves negative chirp with lower phase modulation voltage. The cause for this is believed to be localised heating at the front edge of the phase modulator that for the control device experiences significant optical absorption, with the higher applied modulation voltage and therefore necessarily lower bias point: −2 V.

Conclusion: We have demonstrated how two Franz-Keldysh modulators arranged in a tandem configuration can be used to produce chirp-controlled optical modulation with an effective chirp factor down to −0.86. It is shown how using a long phase modulating section in combination with a simple voltage division scheme to one of the modulator sections can improve the performance of the tandem modulator to <2 dB excess insertion loss and <2 dB degradation of extinction ratio compared to a single section modulator for effective chirp factors down to −0.86.

24 October 2003
Electronics Letters online no: 20040016
doi: 10.1049/el:20040016

L.A. Johansson and L.A. Coldren (*Department of Electrical and Computer Engineering, University of California, Santa Barbara, CA 93106, USA*)

E-mail: leif@ece.ucsb.edu

Y.A. Akulova and G.A. Fish (*Agility Communications, Inc., 600 Pine Ave, Santa Barbara, CA 93117, USA*)

References

1 Akulova, Y.A., *et al.*: 'Widely-tunable electroabsorption-modulated sampled grating DBR laser transmitter', *IEEE J. Sel. Top. Quantum Electron.*, 2002, **8**, pp. 1349–1357
2 Barton, J.S., *et al.*: 'Widely-tunable high-speed transmitters using integrated SGDBRs and Mach-Zehnder modulators', *IEEE J. Sel. Top. Quantum Electron.* (accepted for publication)
3 Claassen, M., Harth, W., and Stegmüller, B.: 'Two-section electroabsorption modulator with negative chirp at low insertion loss', *Electron Lett.*, 1996, **32**, pp. 2121–2122
4 Skogen, E.J., *et al.*: 'A quantum-well-intermixing process for wavelength-agile photonic integrated circuits', *IEEE J. Sel. Top. Quantum Electron.*, 2002, **8**, pp. 863–869
5 Koh, P.C., *et al.*: 'Correlation between dispersion penalty and time-resolved chirp for widely tunable electroabsorption-modulated SGDBR laser across the EDFA gain bandwidth', *IEEE Photonics Technol. Lett.*, 2003, **15**, pp. 1011–1013

High-Speed Optical Frequency Modulation in a Monolithically Integrated Widely-Tunable Laser - Phase Modulator

L.A. Johansson, J.S. Barton and L.A. Coldren
Department of Electrical and Computer Engineering, University of California, Santa Barbara, CA 93106.
Email: leif@ece.ucsb.edu

G.A. Fish
Agility Communications, Inc., 600 Pine Ave, Santa Barbara, CA 93117.

Abstract: A factor of ten improvement of modulation bandwidth, from 2GHz to 20GHz, is demonstrated using phase modulator monolithically integrated to a semiconductor amplifier and a widely-tunable SG-DBR laser. This is achieved by generating optical frequency modulation converted to intensity modulation in an optical ASE filter.
OCIS codes: (250.5300) Photonic integrated devices; (060.2630) Frequency modulation

1. Introduction

Optical frequency modulation (FM) has been considered mainly for analog or coherent links. A frequency modulated, coherently detected link has been shown to exhibit advantages relative to intensity modulated, directly detected links both in terms of SFDR when the received optical power is limited [1] and available SNR [2]. Frequency modulation combined with an optical frequency discriminator has also been considered for analog links [3] in order to reduce the required drive power and therefore to reduce link loss and improve potential link noise figure. In a discriminator-aided FM-link, the SFDR is determined limited by the nonlinear characteristics of the discriminator and can be improved by using special linearized FM discriminators [4]. Recently, increasing interest has also been focused at alternative modulation formats for data transmission when receiver sensitivity, spectral efficiency, constant envelope, or long haul performance is of importance [5].

Common for most FM links is that a directly modulated semiconductor laser diode is used as source because of the relative ease a frequency modulated output can be produced. The drawback of using directly modulated devices is the modulation bandwidth, typically limited to ~10GHz. Optical phase modulators can produce FM at higher modulation frequencies utilizing the transient chirp preceded by signal integration to produce linear frequency modulation. In this paper, we will show how an optical phase modulator can be used to produce optical frequency modulation by operating beyond the conventional *RC*-limited bandwidth of the modulator and how this operating point eliminates the requirement for any preceding signal integration. Combined with an optical frequency discriminator, this modulation scheme also provides a method of greatly extending the available bandwidth of optical modulators. In this work, the modulation bandwidth is increased by a factor of ten.

2. Frequency modulation scheme

An optical phase modulator produces an output optical phase dependent on the applied voltage over the modulator. Within the conventional *RC*-limited bandwidth of the modulator, the phase shift is proportional to the applied signal, ($=V_0$ at DC) and determined by the resistive part of the impedance. The frequency dependence of the phase modulation is given by:

$$\partial\varphi(\omega_m) = \frac{\partial\varphi}{\partial V}\cdot V(\omega_m) = \frac{\partial\varphi}{\partial V}\cdot\frac{1}{j\omega_m RC+1}\cdot V_0(\omega_m) \underset{\omega_m RC>>1}{\approx} \frac{\partial\varphi}{\partial V}\cdot\frac{1}{j\omega_m RC}\cdot V_0(\omega_m) \qquad (1)$$

The phase modulation sensitivity is at lower modulation frequency, ω_m, constant, while at higher frequencies inversely proportional to the modulation frequency. The 3-dB bandwidth is given by the *RC*-constant. Phase modulation can then be converted into amplitude modulation using for example a Mach-Zehnder configuration.

An alternative way of looking at the phase modulator is to consider the frequency modulation at the output of the modulator. The modulator will produce an optical frequency shift, $\delta\omega$, given by:

$$\partial\omega(\omega_m) = -\frac{\partial\varphi}{\partial V}\cdot\frac{\partial V}{\partial t} = -\frac{\partial\varphi}{\partial V}\cdot\frac{1}{j\omega_m RC+1}\cdot\frac{\partial\{V_0(\omega_m)\}}{\partial t} \underset{\omega_m RC>>1}{\approx} \frac{\partial\varphi}{\partial V}\cdot\frac{1}{RC}\cdot V_0(\omega_m) \quad (2)$$

At low modulation frequency, the frequency modulation is proportional to the slope of the modulating signal, which increases as the modulation frequency. At high modulation frequency, the increased slope of the modulating signal is compensated by the capacitive roll-off, and the frequency response will be that of a high-pass filter with a 3-dB cut-off frequency again given by the *RC*-constant. Above the 3-dB point, the frequency dependence of the FM is flat. For a very long modulator, the increased capacitance will be compensated for by increased phase modulation sensitivity, leaving the FM sensitivity constant, according to eq. 2, the low-frequency cut-off will however be improved. The frequency modulated signal can be demodulated in a number of ways, including coherent detection schemes [2] or FM to IM conversion using an optical frequency discriminator [4,6].

When using demodulation by FM to IM conversion, there is a tradeoff in required modulation efficiency and bandwidth. The spectral bandwidth of an FM signal is given by Carson's rule, $B_{FM} \approx 2(\delta\omega+\omega_m)$. The modulation bandwidth is limited by the response of the discriminator, that can only sustain a high slope sensitivity over a limited frequency range. Meanwhile, the instantaneous frequency shift required to achieve a high modulation depth is similarly determined by the discriminator response. A relative comparison of phase modulation and the corresponding frequency modulation of a modulator can be obtained by considering the modulation voltage required to switch the output between maximum and minimum transmission, the equivalent V_π. For frequency modulation, the equivalent V_π is given by the voltage needed to generate a frequency shift of $\delta\omega_\pi$, corresponding to maximum and minimum transmission through the discriminator. From the bandwidth-efficiency limit outlined above, $\delta\omega_\pi$ also roughly corresponds to the bandwidth limit. Assuming a Mach-Zehnder-type discriminator chosen to achieve a FM bandwidth n times that of the modulator *RC*-limit. Inserting this into equation 2, we obtain the equivalent V_π:

$$V_\pi = \frac{n\pi}{\partial\varphi/\partial V_{\max}} \quad (3)$$

The factor of π in the numerator results from the sinusoidal response of the Mach-Zehnder discriminator. The expression for V_π corresponds to the bandwidth-modulation efficiency limit of the corresponding MZ modulator that is obtained by changing the length of the modulator arms, assuming the first order approximation of linear dependency of capacitance to modulator length.

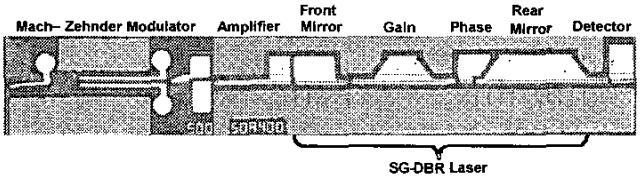

Fig. 1. Outline of SG-DBR laser integrated with an SOA and a Mach-Zehnder modulator.

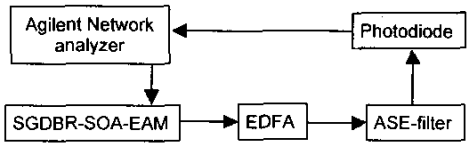

Fig. 2. Outline schematic of experimental Arrangement.

3. Experiment

The monolithically integrated device is similar to that described in [7], where a sampled-grating DBR laser is integrated with a semiconductor optical amplifier and a Mach-Zehnder modulator, all on a single InP-substrate. An outline of the device is shown in Fig. 1. The modulator electrodes are 500μm long with a 97μm long 1x2 MMI coupler at the laser input and a 170 μm long 2x2 MMI to the waveguide outputs. The total device length is then 3400um long consisting of the 1.75mm SGDBR 0.4mm SOA and 1000um MZ device with integrated curved waveguide passive regions at the facets.

Figure 2 shows a schematic of the experimental setup. An Agilent 50GHz network analyzer was used to modulate the phase modulator. For characterization of phase modulation performance, the MZ modulator is biased for maximum slope sensitivity, while for characterization of frequency modulation, one arm of the MZ modulator is reverse biased for absorption such that the output consists only of the output of the second arm. The output of the device is then amplified to compensate for the filter insertion loss. After the EDFA, a 0.4nm optical filter is used, partly to remove the ASE noise and partly to provide an optical frequency dependent element for discriminator FM to IM conversion. The IM signal is then detected by a U^2T photodiode and the output signal is fed back to the Agilent network analyzer.

Figure 3 shows the measured bandwidth using phase modulation and frequency modulation of one arm of the MZ modulator. The phase modulator is unmatched with a bandwidth of 2GHz. The bandwidth of a 50Ω-matched, equally long modulator is on the order of 5GHz. Switching off the output of the second arm, the output consists of the phase/frequency modulated output of the first arm of the MZ-modulator. Tuning the optical filter to maximum slope sensitivity at center frequency, the bandwidth of the modulator is increased by a factor of ten to 20GHz. The measured bandwidth corresponds well to what is expected from the filter FWHM bandwidth; 0.4nm ≈ 50GHz at 1566.4nm, the emission wavelength of the SG-DBR laser. A wider bandwidth optical filter will sustain a wider frequency swing and therefore produce a wider modulation bandwidth, though the efficiency of the FM to IM conversion will be compromised.

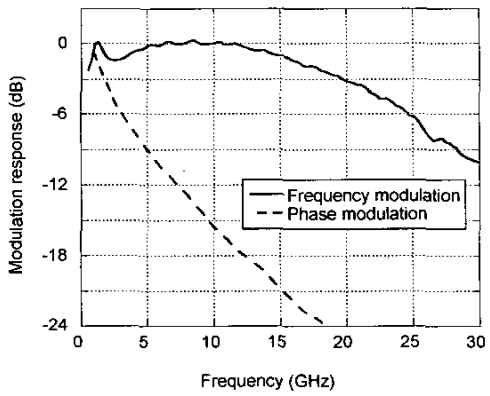

Fig. 3. Measured bandwidth for phase modulation converted to intensity modulation in the Mach-Zehnder modulator and for frequency modulation converted to intensity modulation using an optical frequency discriminator.

4. Summary

In this paper we have showed how an optical phase modulator monolithically integrated to a semiconductor amplifier and a widely-tunable SG-DBR laser can be used to produce optical frequency modulation at modulation frequencies beyond the *RC*-limited bandwidth of the phase modulator. Combined with FM to IM conversion using an optical frequency discriminator, the available modulation bandwidth is limited to frequencies between the conventional *RC*-limit on the low frequency side and the maximum frequency swing accommodated by the frequency discriminator. Further, it is shown how the available bandwidth-modulation efficiency product is comparable to that of using phase modulation to intensity modulation conversion in a Mach-Zehnder configuration. The bandwidth-modulation efficiency product can be improved by using a coherent detection scheme, instead of FM to IM conversion. Finally, the described modulation scheme is demonstrated modulating one electrode of a Mach-Zehnder modulator integrated with an SG-DBR laser and an SOA. The available FM bandwidth is shown to increase by a factor of ten, from 2GHz to 20GHz, compared to that of the Mach-Zehnder modulator. The FM bandwidth can be further increased by selecting a frequency discriminator with lower slope sensitivity at the price of lower conversion efficiency.

5. References

[1] R.F. Kalman, J.C. Fan and L.G. Kazovsky, "Dynamic range of coherent analog fiber-optic links," IEEE J. Lightwave Technol., 12, pp.1263-1277, (1994).

[2] B. Cai and A.J. Seeds, "Optical frequency modulation links: Theory and experiments," IEEE Trans. Microwave Theory Tech. **45**, pp 505-511 (1997).

[3] Qiangsheng Xiang, Yang Zhao and Fow-Sen Choa, "A high-performance RF-lightwave transmitter for analog fiber links," IEEE LEOS Annual Meeting 2000, Vol. 1, pp. 13-16 (2000).

[4] Xiaobo Xie, J. Khurgin, Jin Kang and Fow-Sen Choa, "Ring-assisted frequency discriminator with improved linearity," IEEE Photon. Technol. Lett., **14**, pp 1136-1138 (2002).

[5] A. H. Gnauck, G. Raybon, S. Chandrasekhar, J. Leuthold, C. Doerr, L. Stulz, A. Agrawal, S. Banerjee, D. Grosz, S. Hunsche, A. Kung, A. Marhelyuk, D. Maymar, M. Movassaghi, X. Liu, C. Xu, X. Wei, and D. M. Gill, "2.5 tb/s (64×42.7 Gb/s) transmission over 40×100 km NZDSF using RZ-DPSK format and all-raman-amplified spans," Proc. OFC, 2002, Postdeadline Paper FC2.

[6] G. Fiksman, R. Gross, J. Fan and L. Kazovsky, "Performance optimization of directly modulated FM-SCM systems with optical discriminator," IEEE Photon. Technol. Lett., **5**, pp 845-848 (1993).

[7] J.S. Barton, E.J. Skogen, M.L. Mašanović, S.P. Denbaars, and L.A. Coldren, "Widely-tunable high-speed transmitters using integrated SGDBRs and Mach-Zehnder modulators," to be published in IEEE J. Selec. Top. Quantum Electron.

10 Gb/s Mach-Zehnder modulator integrated with widely-tunable sampled grating DBR Laser

Y. A. Akulova, G. A. Fish, P. Koh, P. Kozodoy, M. Larson, C. Schow, E. Hall, H. Marchand, P. Abraham, L. A. Coldren
Agility Communications, Inc., 475 Pine Ave, Santa Barbara, CA 93117
yakulova@agility.com

Abstract: We report on a sampled grating DBR laser monolithically integrated with a Mach-Zehnder modulator and a semiconductor optical amplifier. Transmission over 100 km of standard fiber at 10 Gb/s is demonstrated across 30 nm tuning range.

OCIS codes: (250.5300) Photonic integrated circuits; (060.2330) Fiber optics communications

1. Introduction

A compact, high-performance widely-tunable integrated laser/modulator chip is a key component of a tunable transmitter that can dramatically lower the barriers to deployment and operation of high capacity DWDM networks. Several tunable laser technologies with integrated electroabsorption (EA) modulator operating at a bit rate of 2.5 Gb/s and beyond have been demonstrated [1-3]. Integrated transmitters based on EA-modulators although successfully deployed in metropolitan networks have received only limited acceptance in long-haul transmission systems at 10 Gb/s. The main limitations of the EA-modulator are inherent wavelength dependence of extinction ratio (ER) and chirp and trade-off between these characteristics and insertion loss. In contrast to EA-modulators, Mach-Zehnder (MZ) modulators offer the capability of precise control over chirp and extinction ratio over wide wavelength range without introducing excess loss [4]. Co-packaging of a tunable laser with a lithium niobate or III-V MZ modulator is being widely pursued by component manufactures to minimize cost and size of tunable transmitters [5]. The advantage of the co-package approach is the possibility to select laser and modulator chip characteristics independently and to ensure good optical and electrical isolation between the laser and modulator. However, further reduction of package complexity, cost, and size is achievable only through monolithic integration of a laser and a MZ modulator. Reports on a monolithically integrated III-V MZ modulator with a very narrowly-tunable gain-coupled DFB laser have demonstrated feasibility of integration and acceptable system performance at 2.5 and 10 Gb/s [6].
In this paper we discuss the design and performance of a widely tunable transmitter chip based on a Sampled Grating Distributed Bragg Reflector (SG-DBR) laser monolithically integrated with a semiconductor optical amplifier (SOA), and a Mach-Zehnder modulator (MZM). Negative and zero chirp of the transmitted signal were demonstrated by adjusting the drive voltages for two arms of MZM. Error-free transmission at 10 Gb/s for 100 km of standard single mode fiber over 30 nm wavelength range has been demonstrated for the first time for a widely-tunable laser monolithically integrated with a modulator.

2. Device design and fabrication

As illustrated in Fig. 1, the device consists of a four-section SG-DBR laser, an SOA, and a MZM, all integrated on the same InP chip. The integrated SOA compensates on-state modulator loss and cavity losses caused by free carrier absorption in the tuning sections and allows wavelength independent power leveling, beam blanking during wavelength switching, and variable optical attenuator functionality. The MZ modulator consists of two multi-mode interference (MMI) sections with curved waveguides and 400 um long lumped electrodes. The integration of the laser and SOA active regions with the tuning and modulator sections of the device has been accomplished by using an offset quantum-well structure [7]. In this simple integration technology the active region of the modulator uses the same bulk quaternary waveguide as the tuning sections of the laser. The composition of the bulk waveguide can be optimized to achieve high tuning efficiency for the laser and a target V_π over the required wide spectral bandwidth for the modulator. The device is fabricated using shallow-ridge technology to ensure low optical reflections as compared to the deep-ridge structures due to reduced index step between optical waveguides and MMI

sections [8]. An angled waveguide and wide-band anti-reflection coating at the output of the device were used to suppress the facet feedback.

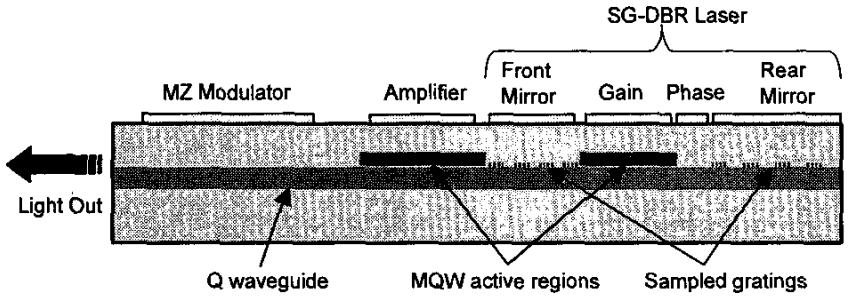

Fig. 1. Schematic of SG-DBR laser integrated with SOA and MZ modulator.

3. Results and discussion

The fabricated devices were mounted on ceramic carriers with co-planar waveguides and integrated matching resistors. For transmission measurements the chip-on-carrier was packaged into a cooled butterfly module with a co-planar RF input.

The output power vs. wavelength for a SG-DBR-SOA-MZM chip is shown in Fig. 2a). For this measurement the nominally π-phase shifted MZM is biased to produce differential phase shift of 0 radians between the two arms. The integrated chips are capable of producing more than 15 mW of power across 40 nm tuning range in the C-band. Figure 2b) shows normalized transmission characteristics for a packaged SG-DBR-SOA-MZM chip at three wavelength across C-band. DC ER in excess of 20 dB is achieved with less than 3.3 V. In single-ended drive configuration RF ER of 12 dB was measured across 40 nm tuning range with less than 3 V peak-to-peak modulation voltage (Fig. 2c).

The key for achieving uniform transmission performance of the integrated SG-DBR-SOA-MZM transmitter over wide wavelength range is in eliminating optical and electrical crosstalk and precise control of the transient chirp of the modulator. Measurements of the time-resolved chirp characteristics of the integrated chips confirmed that extrinsic chirp components due to optical feedback or electrical crosstalk are completely eliminated. The remaining chirp component is transient chirp determined by a MZM design and drive conditions. The transient chirp of p-i-n InP MZ modulator is a function of electrooptic properties of active material, splitting ratio of the two MMI sections, the differential phase shift between two arms, and the format of the modulation voltages applied to each arm of the modulator [9]. These features provide flexibility of optimizing device performance for zero or negative chirp over wide wavelength range. Figure 2c) shows wavelength dependence of the effective α-parameter extracted from the time-resolved chirp characteristics in a 3 dB region of the most transparent state of the modulator in single-ended drive configuration. Uniform chirp of -0.74+/- 0.1 is maintained across the tuning range.

Figure 3a) shows output and transmitted eye diagrams for dual- and single-ended drive conditions at 10 Gb/s for a π-shifted MZM. Maximum peak-to-peak modulation voltage for 12 dB RF ER across the C-band is 1.5 and 3 V for dual- and single-ended drive, respectively. The dual-drive condition results in "zero" chirp configuration, while single-ended operation results in "negative" chirp. Wide open eye diagrams after 50 km ("zero" chirp) and 100 km ("negative" chirp) of standard non-dispersion shifted fiber indicate that the integrated chips are capable of meeting stringent requirements for 10 Gb/s transmission. The back-to-back and 100 km BER curves were measured for negative chirp configuration for three wavelength across C-band. The lowest wavelength for this measurement was limited to 1535 nm by the tunable bandpass filter. The BER data presented in Fig. 3 b) shows error free transmission for 1600-1800 ps/nm dispersion for 1535-1563 nm wavelength range. Evaluation of dispersion penalty for longer transmission distances is currently in progress.

4. Summary

In summary, we have demonstrated a widely-tunable, 10 Gb/s transmitter chip based on a SG-DBR laser monolithically integrated with a SOA and MZ modulator. *RF* extinction ratio > 12 dB with less than 3 V modulation

voltage and negative chirp across a 40 nm tuning range have been achieved. Error-free transmission at 10 Gb/s has been demonstrated for 100 km of standard single mode fiber.

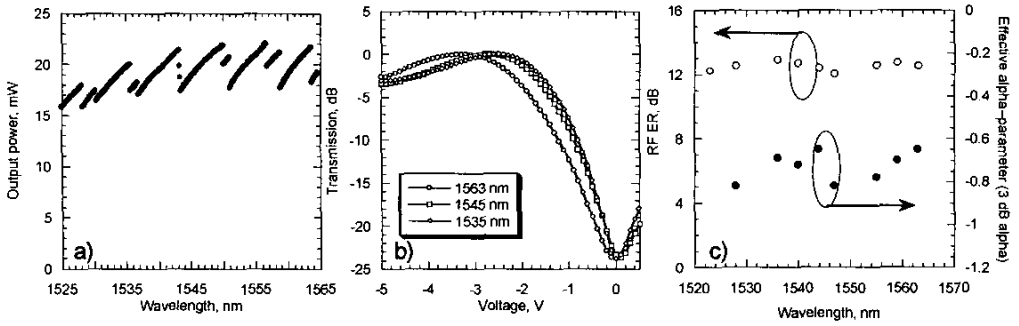

Fig. 2. a) Unleveled SG-DBR-SOA-MZM output power across the tuning range. b) Normalized transmission characteristic for three wavelengths. c) RF ER and 3 dB alpha parameter in single-ended drive configuration across the tuning range.

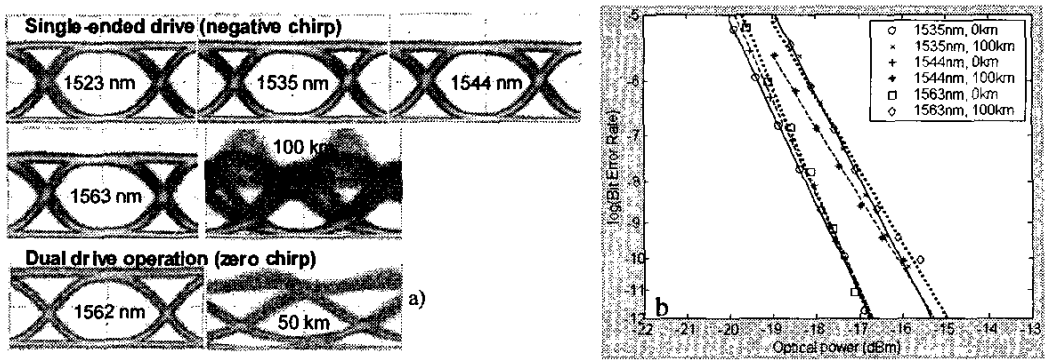

Fig. 3. a) Output eye diagrams and eye after fiber in single and dual drive configurations. b) Bit error rate curves for 0 and 100 km of standard single-mode fiber spans for three different wavelengths (10 Gb/s NRZ, 2^{21}-1 PRBS).

5. References

[1] J.E. Johnson, L.J.-P. Ketelsen, D.A. Ackerman, Zhang Liming, M.S. Hybertsen, K.G. Glogovsky, C.W. Lentz, W.A. Asous, C.L. Reynolds, J.M. Geary, K.K.; Kamath, C.W. Ebert, M. Park, G.J. Przybylek, R.E. Leibenguth, S.L. Broutin, and J.W. Stayt, Jr, "Fully stabilized electroabsorption-modulated tunable DBR laser transmitter for long-haul optical communications ", IEEE J. Select. Topics Quantum Electron., **7**, 168 -177 (2001).

[2] T. Marimoto, K. Yashiki, K. Kudo, and T. Sasaki, "Wavelength-selectable microarray light sources for DWDM photonics networks", IEICE Trans. Electron., **E85-C**, 982-989 (2002).

[3] Y.A. Akulova, G.A. Fish, Ping-Chick Koh, C.L. Schow, P. Kozodoy, A.P. Dahl, S. Nakagawa, M.C. Larson, M.P. Mack, T.A. Strand, C.W. Coldren, E. Hegblom, S.K. Penniman, T. Wipiejewski, L.A. Coldren, "Widely tunable electroabsorption-modulated sampled-grating DBR laser transmitter", IEEE J. Select. Topics Quantum Electron., **8**, 1349 -1357 (2002).

[4] J.S. Barton, E.J. Skogen, M.L. Masanovic, S.P. DenBaars, L.A. Coldren, "Tailorable chirp using integrated Mach-Zehnder modulators with tunable sampled grating distributed Bragg reflector lasers", Proc. IEEE 18th International Semiconductor Laser Conference, 49 –50 (2002).

[5] R. A. Griffin, R. I Johnstone, R. G. Walker, J. Hall, S. D. Wadsworth, K. Berry, A. C. Carter, M. J. Wale, J. Hughes, P. A. Jerram, and N. J. Parsons, "10Gb/s optical differential quadrature phase shift key (DQPSK) transmission using GaAs/AlGaAs Integration", OFC'02, FD6-1 (2002).

[6] C. Rolland, "InGaAsP-based Mach-Zehnder modulators for high-speed transmission systems", OFC Technical Digest, 283 –284 (1998).

[7] B. Mason, G. A. Fish, S. P DenBaars, and L. A. Coldren, "Widely tunable sampled grating DBR laser with integrated electroabsorption modulator", IEEE Photn. Technol. Lett., **11**, 638-40 (1999).

[8] S. Lovisa, N. Bouche, H. Helmers, Y. Heymes, F. Brillouet, Y. Gottesman, K. Rao, "Integrated laser Mach-Zehnder modulator on indium phosphide free of modulated-feedback", IEEE Photon. Technol. Lett. , **13**, 1295 -1297 (2001).

[9] C. Lawetz, J.C. Cartledge, C. Rolland, J. Yu, "Modulation characteristics of semiconductor Mach-Zehnder optical modulators", J. of Lightwave Technol., **15**, 697-703 (1997).

Wavelength Agile, Integrated Analog Optical Transmitters

G. A. Fish, Y. A. Akulova, and L. A. Coldren
Agility Communications, Inc., 475 Pine Ave, Santa Barbara, CA 93117
1-(805) 690-1722 / gfish@agility.com

L. A. Johansson, L. A. Coldren
Department of Electrical and Computer Engineering University of California, Santa Barbara, CA 93106
1-(805) 893-4543 / leif@ece.ucsb.edu

Abstract

We report on analog modulation characteristics of a widely-tunable sampled grating DBR laser monolithically integrated with an electroabsorption or Mach-Zehnder modulators and a semiconductor optical amplifier. A sub-octave SFDR of 125-127 dB/Hz4/5 and a broadband SFDR of 103-107 dB/Hz2/3 limited by third order intermodulation products is demonstrated over a 1528 to 1573 nm wavelength range.

1. INTRODUCTION

Analog optical links have found applications areas such as wireless over fiber or antenna remoting for radar applications. In both cases, the optical link provides a low loss, wide band with medium, transparent to modulation format. The antenna units can be simplified, while system complexity can be located at a centralized location. The merging of WDM and wireless over fiber technologies will further enhance system reconfigurability and capacity, particularly for wireless over fiber applications [1]. Signal routing will enable dynamic allocation of radio resources and increased overall system capacity.

In this work, we have investigated the performance of an integrated photonic transmitter module based on a monolithically integrated InP chip comprising of a sampled-grating distributed Bragg grating (SG-DBR) laser, a semiconductor optical amplifier (SOA), and an electroabsorption modulator (EAM) or a Mach-Zehnder modulator (MZM), for high-performance analog optical link application. The paper is structured as follows. In section 2, a brief overview of the SG-DBR laser platform that these analog transmitters are based upon is presented. In section 3.2, the performance of transmitter including an EAM is reviewed. The performance of transmitters including a MZM is summarized in section 3.2, and the summary, section 4 gives a brief comparison of the performance of the two types of transmitters.

2. DEVICE DESIGN AND FABRICATION

As illustrated in Figure 1, the device consists of a four-section SG-DBR laser, an SOA, and an EAM or MZM, all integrated on the same InP chip. Formed by sampling (periodically blanking) front and back grating mirror sections longitudinally integrated in-plane with active and phase tuning sections, the SG-DBR lasers rely on refractive index tuning through current injection combined with the vernier effect for wide (>40 nm) wavelength coverage [2]. The integration of the laser and SOA active regions with the tuning and modulator sections of the device has been accomplished by using an offset quantum-well structure. In this simple integration technology the active region of the modulator uses the same bulk quaternary InGaAsP waveguide as the tuning sections of the laser. The composition of the bulk waveguide can be optimized to achieve high tuning efficiency for the laser and a target Vp over the required wide spectral bandwidth for the modulator. The developed integration technology is compatible with reliable, low cost, wafer-scale InP manufacturing process. The monolithic integration of laser and modulator also results in reduced cost and complexity of the package assembly [3].

3. DEVICE CHARACTERISTICS

3.1 EAM Transmitter

The spurious-free dynamic range (SFDR) of the packaged SG-DBR-SOA-EAM device was measured at 0.5 GHz using two-tone modulation at 1 MHz offset of between -5 dBm to 8 dBm modulation power each. Figure 2a shows the broadband and sub-octave spurious-free dynamic range, both for 1Hz and 1MHz noise bandwidth. The broadband SFDR is taken at 1552 nm, 180mA bias current to gain section and SOA and at the bias point of minimum second order distortion. The noise level is –157 dBm/Hz, limited by shot noise and laser RIN. The SFDR limited by second order distortion is 97.19 dB in 1 Hz bandwidth and the SFDR limited by third order distortion is 106.09 dB in 1 Hz

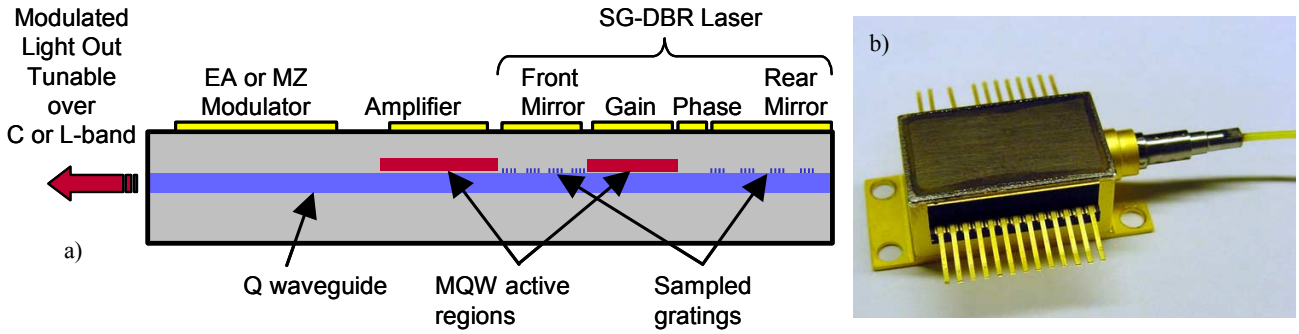

Figure 0 a) Schematic cross-section of an SGDBR-SOA-Modulator chip (chip dimensions 3x0.5 mm2). b) Packaged widely-tunable optical transmitter (package size 1x0.5x0.5 in3).

bandwidth, corresponding to 66.09 dB in 1 MHz bandwidth. The broadband SFDR was also measured at several wavelengths over the tuning range of the laser. At each wavelength the dc bias on the modulator was adjusted to the minimum second order distortion. The SFDR remains within a 103-107 dB/Hz2/3 range limited by third order intermodulation products, dominant for noise bandwidths above 1MHz, or 95-98 dB/Hz1/2 range limited by second order intermodulation products. The sub-octave SFDR is taken at 1552 nm, 180mA bias current to gain section, 120 mA SOA bias and at the bias point of minimum third order distortion (Figure 2b). The noise floor is mainly limited by shot noise. The SFDR is 126.28 dB in 1 Hz bandwidth and remains within a 125-127 dB/Hz4/5 range, all limited by fifth order intermodulation products over the tuning range of the laser. RF gain of +10.5 dB and noise figure of 5.07 dB were simultaneously measured for pre-amplified optical link.

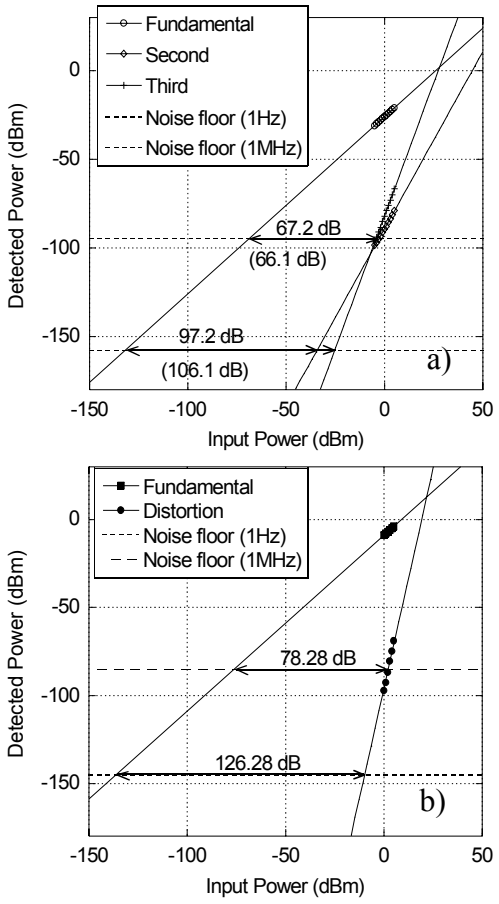

Figure 1 a) Power of noise floor, fundamental, second and third order intermodulation products at –1.1V EAM bias. Broadband SFDR is shown in 1Hz and 1MHz bandwidth. b) Power of noise floor, fundamental and third order intermodulation products at –2.5 V EAM bias. Sub-octave spurious-free dynamic range is also shown in 1Hz and 1MHz bandwidth.

The spurious-free dynamic range (SFDR) of the device is measured using two-tone modulation at 1 MHz offset of between -5 dBm to 8 dBm modulation power each.

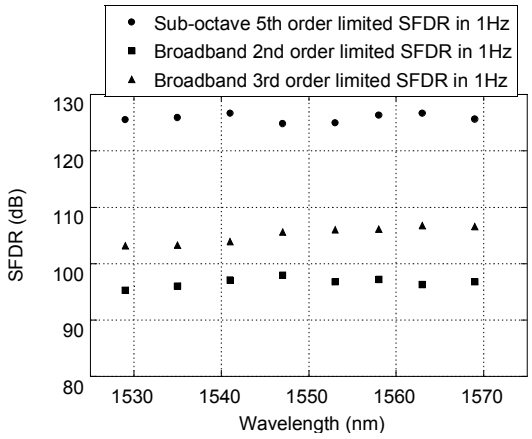

Figure 2 Measured sub-octave and broadband spurious-free dynamic rage, left scale, normalized to 1 Hz bandwidth for different wavelengths. Sub-octave SFDR limited by fifth shown is relative effect on SFDR from the RIN level of the order intermodulation products and broadband SFDR limited source.

Figure 1 a) and b) show the broadband and sub-octave spurious-free dynamic range, both for 1Hz and 1MHz noise bandwidth. The broadband SFDR is taken at 1552 nm, 180mA bias current to gain section and SOA and at the bias point of minimum second order distortion. The noise level is –157 dBm/Hz, limited by shot noise and laser RIN. The SFDR limited by second order distortion is 97.19 dB in 1 Hz bandwidth and the SFDR limited by third order distortion is 106.09 dB in 1 Hz bandwidth, corresponding to 66.09 dB in 1 MHz bandwidth. Figure 2 shows the broadband SFDR over the tuning range of the laser. The SFDR remains within a 103-107 $dB/Hz^{2/3}$ range limited by third order intermodulation products, dominant for noise bandwidths above 1MHz, or 95-98 $dB/Hz^{1/2}$ range limited by second order intermodulation products. The sub-octave SFDR is taken at 1552 nm, 180mA bias current to gain section, 120 mA SOA bias and at the bias point of minimum third order distortion. The noise floor is mainly limited by shot noise. The SFDR is 126.28 dB in 1 Hz bandwidth and remains within a 125-127 $dB/Hz^{4/5}$ range, all limited by fifth order intermodulation products over the tuning range of the laser, Figure 2.

3.2 Mach-Zehnder Transmitter

The Mach-Zehnder modulator has a number of advantages compared to EA modulators. First of all, the RF link gain of a EA modulated optical link becomes limited by the absorbed photocurrent [4]. MZ modulators do not have this limitation, being based on interferometric modulation. Second, by choosing inverting, non-inverting or a combined push-pull modulation, the modulator chirp can be controlled from positive to negative values. In terms of linearity, Mach Zehnder modulators have one disadvantage. With its sinusoidal response, the third order infliction points appear at the same bias point as zero slope sensitivity, limiting the available sub-octave SFDR [5]. Figure 1 shows a simple schematic of an SG-DBR laser integrated to an SOA and a Mach-Zehnder modulator. Since the MZ modulator is defined in the same material and with the same fabrication steps as the SG-DBR laser and SOA, the fabrication process is not

much more complex than for the SG-DBR laser alone. The composition of the bulk waveguide can be optimized to achieve high tuning efficiency for the laser and a target V_p over the required wide spectral bandwidth for the modulator. The length of the electrodes of the Mach-Zehnder is in the 300μm to 700 μm range.

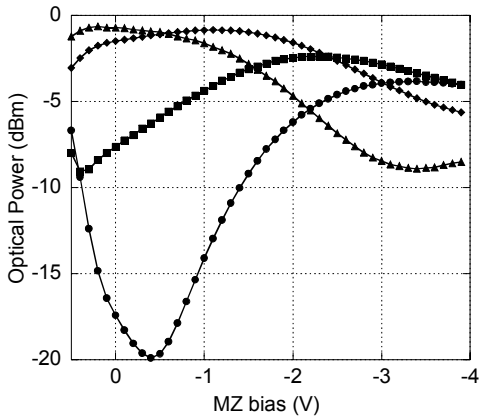

Figure 3 Typical extinction curves for various differential MZ phase settings.

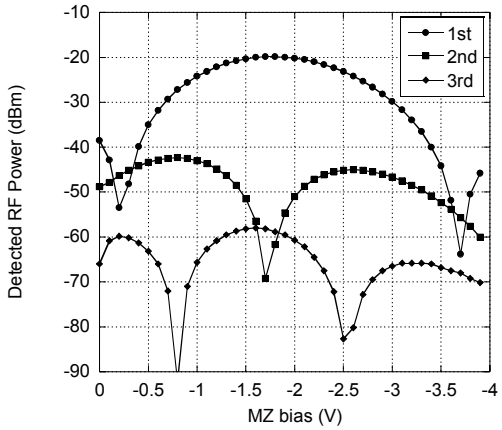

Figure 4 Detected RF power of fundamental and intermodulation products for 0 dBm modulation power.

Figure 3 shows a typical set of extinction curves for different values of phase difference between the arms of the Mach-Zehnder. In order to achieve high extinction, both the phase and the amplitude of the field passing through the arms of the Mach-Zehnder need to be matched. When both arms are biased around 0V, good extinction is achieved by design. When the phase offset is tuned to a different value, the available extinction ratio is obtained away from 0V and is degraded. The reason is the onset of Franz-Keldysh absorption in the bulk material. This can be a problem for digital applications and is the reason that it has been designed for good extinction around 0V. For analog applications, the altered response of the Mach-Zehnder can be taken advantage of in order to enhance the SFDR of the modulator. This is illustrated in Figure 4 for 300μm electrode length, where the detected power of fundamental, second and third order intermodulation products are plotted as a function of MZ bias. As expected, the points of minimum second order distortion coincides with the point of maximum slope efficiency. However, unlike the typical Mach-Zehnder modulator, the points of maximum second order distortion, and therefore minimum third order distortion, do not coincide with minimum power of the fundamental. Therefore, by tuning the MZ bias point for minimum third order distortion, there is only about 3.3 dB penalty in the RF power of the fundamental, and optimized linearity for sub-octave applications is obtained. At this bias point, the sub-octave SFDR is 107.5 dB/Hz$^{2/3}$, limited by third order intermodulation products as shown in Figure 6. The broadband SFDR is obtained by choosing the bias point where second order distortion has a minimum and is 92.8 dB/Hz$^{2/3}$, when limited by second order distortion or 103.6 dB/Hz$^{2/3}$, when limited by third order distortion products, as show in Figure 7. In both cases, the noise floor was limited mainly by shot noise. It is worth noting that even though the fiber coupled output power of the MZ-devices, a peak 2mW, was much smaller than for the EA-devices, a peak 10mW, the broadband SFDR was comparable for both devices. MZ-devices with similar output power as the EA-devices should deliver improved broadband SFDR.

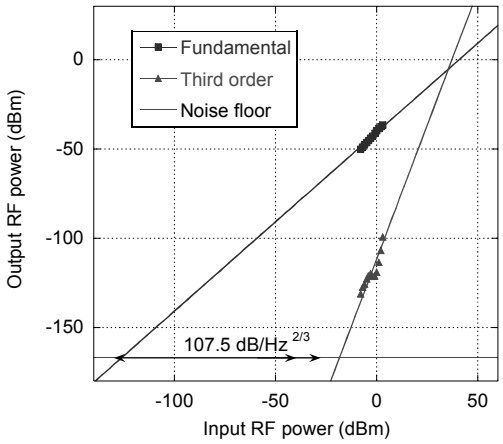

Figure 5 Measured power of noise floor, fundamental and 3rd order intermodulation products at 1547 nm.

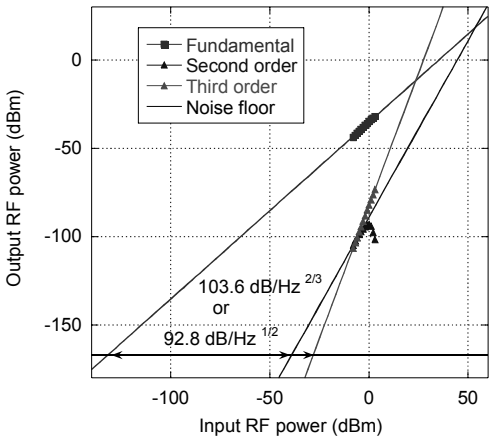

Figure 6 Measured power of noise floor, fundamental, 2nd and 3rd order intermodulation products at 1547 nm.

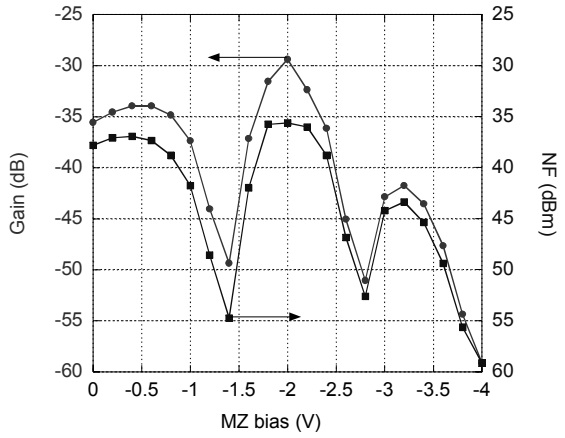

Figure 7 MZ-modulated link gain and noise figure as a function of electrode bias point.

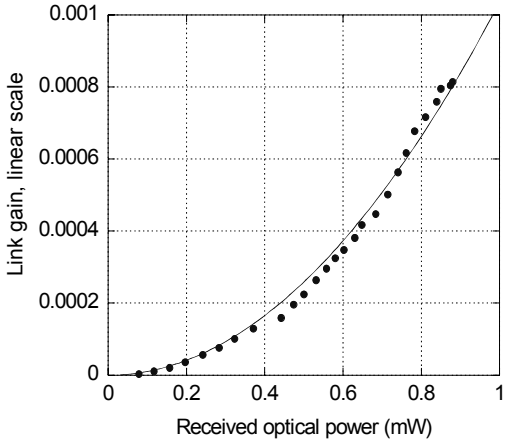

Figure 8 MZ-modulated optical link gain as a function of received optical power.

A 700μm electrode MZ-device was used for a link experiment, measuring link gain and noise figure. The longer electrode length was chosen to improve gain and noise figure in the absence of any preamplification. The link gain peaks at slightly above –30 dB, with an attributed noise figure of just below 35 dB, as shown in Figure 7. Again, despite that the peak output power is about five times lower for the MZ-devices than for the EA-devices, the link noise figure is comparable, mainly as a result of the steeper slope sensitivity of the long electrode MZ. A second contributing reason is the fact that this is an interferometric modulator, not as severely affected by that the absorbed photocurrent that had such a drastic impact on the response of the EA-devices. In fact, plotting the link gain on a linear scale as a function of received optical power (Figure 8), an almost perfect square relationship between link gain and power is obtained, indicating no compression of the modulator response with optical power. This relationship may be extrapolated at higher output power, such that a MZ-device with 10mW peak output power would have superior link performance of the corresponding EA-device.

4. SUMMARY

In this paper, SG-DBR laser based devices integrated to an SOA and either an electroabsorption modulator or a Mach-Zehnder modulator have been investigated for application as an analog transmitter. The performance has been evaluated in terms of spurious-free dynamic range, conversion efficiency and link noise figure. Using the EA device, a sub-octave SFDR of 126.3 dB/Hz4/5 and a broadband SFDR of 106.1 dB/Hz2/3 limited by third order intermodulation products or 97.2 dB/Hz1/2, limited by second order intermodulation products is measured. A link gain up to –20.7 dB and noise figure up to 32.1 dB is also measured. For the MZ-device, the sub-octave SFDR was slightly worse, 107.5 dB/Hz2/3, mainly determined by the lower output power of the MZ-device and the third order power dependence of the distortion. The broadband SFDR was comparable to the EA-modulator at 103.6 dB/Hz2/3 limited by third order intermodulation products or 92.8 dB/Hz1/2, limited by second order intermodulation products. A link gain of –30 dB and noise figure of 35 dB is measured. These numbers would greatly benefit from higher output power as the MZ-modulator is not limited by photocurrent effects.

5. ACKNOWLEDGEMENTS

This work was in part funded by DARPA/MTO under the RFLICS program and in part under the CS-WDM program.

6. References

[1] C. Lim, A. Nirmalathas, M. Attygalle, D. Novak, R. Waterhouse, "The merging of a WDM fiber-radio backbone with a 25 GHz WDM ring network," *2003 IEEE MTT-S Microwave Symposium Digest*, vol.1, pp. 273 -276, June 8-1,3 2003.

[2] V. Jayaraman, Z.-M. Chuang, L. A. Coldren, "Theory, Design, and Performance of Extended Tuning Range Semiconductor Laser with Sampled Grating", *IEEE J. of Quantum Electron*., 29, pp. 1824 –1834, 1993.

[3] Y. A. Akulova, G. A. Fish, P. C. Koh, C. Schow, P. Kozodoy, A. Dahl, S. Nakagawa, M. Larson, M. Mack, T. Strand, C. Coldren, E. Hegblom, S. Penniman, T. Wipiejewski, and L. A. Coldren, "Widely-Tunable Electroabsorption-Modulated Sampled Grating DBR Laser Transmitter", *IEEE Journal on Selected Topics in Quantum Electronics*.8, pp. 1349-1357, 2002.

[4] G.L. Li, P.K.L. Yu, W.S.C. Chang, K.K. Loi, C.K. Sun and S.A. Pappert, "Concise RF equivalent circuit model for electroabsorption modulators," *Electron. Lett.* 36, pp. 818-820, 2000.

[5] M. Farwell, W. Chang, and D. Huber, "Increased linear dynamic range by low biasing the Mach-Zehnder modulator," *IEEE Photon. Technol.Lett*., 5 , pp. 779-782, Jul. 1993.

7. BIBLIOGRAPHY (IES)

None available at the time of submission.

Proc. GOMACTech 2004, paper no. 9.4, Monterey, CA (March 15-18 2004)

High-efficiency 'receiverless' optical interconnects

Larry A. Coldren, University of California, Santa Barbara, CA 93106
Joe C. Campbell, University of Texas, Austin, TX

The objective of this work is to develop new chip-to-chip optical interconnect architectures using novel transmitter and receiver modules for terabit data throughput in multi-chip modules. High-efficiency, high-speed, high-power photodetectors and integrated surface-emitting laser-modulators are being explored to enable minimal or no additional electronics at the receiver.

On the transmitter side we are developing high-efficiency, high-power, ~980 nm, integrated in-plane laser-modulator arrays for this architecture. Quantum-well intermixing (QWI) is being used to define the grating and modulator regions as well as for lateral carrier confinement. New levels of power efficiency are expected in a relatively small footprint. The QWI can provide simultaneous optimization of the gain and modulator characteristics for high power (~20mW), modulation bandwidth (~40GHz), and low modulation voltage. CAIBE etched 45-degree facets at the end of the modulator will be explored in the future for reduced back reflections and vertical emission through the substrate. In this case monolithically integrated microlenses on the backside of the substrate will also be investigated. Comparisons of this architecture to alternative VCSEL approaches will be given.

"Digital" receiver circuits in which the photodiodes are directly connected to the logic circuitry are being developed. In order to generate the required drive voltage, it is necessary for the photodiode to operate at higher input optical power levels than telecommunication optical receivers. Conventional photodiode structures exhibit saturation at high frequencies. Recently, we have designed and characterized a new photodiode structure that has achieved a record current-bandwidth product of >1000mA·GHz to above 40 GHz. These photodiodes are uniquely positioned to directly drive digital logic circuits with no degradation in the frequency response.

As illustrated in Fig. 1, an in-plane surface-emitting laser-modulator (IPSEL-Mod) array having elements with short cavities and highly-reflecting rear mirrors for high efficiency, high power, and high speed at relatively high temperatures is being developed. Wavelengths of both 980nm (GaAs-based) and 1300 nm (InP-based) are being will investigated. Also illustrated in Fig. 1 are backside microlenses. These have been previously developed on the backside of VCSELs and will be explored in the future. Elliptical shapes will be explored for collimation into circular beams.

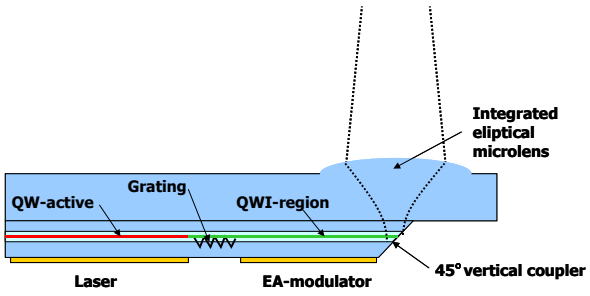

Figure 1. In-plane surface-emitting laser with integrated EA-modulator (IPSEL-Mod).

In the photodetector high saturation current at high bandwidth is required. In order to reduce the space charge effect and thus increase the operating current , we have developed an $In_{0.53}Ga_{0.47}As$ photodiode with a partially depleted absorber (PDA). The primary motivation for the PDA structure is charge balance in the depletion region, which reduces the space-charge effect. A schematic cross section and initial frequency response data is shown in Figure 2. Unlike conventional, long-wavelength PINs, for the PDA structure, the $In_{0.53}Ga_{0.47}As$ depletion region is sandwiched between p-type and n-type undepleted $In_{0.53}Ga_{0.47}As$ absorbers. The doping in the undepleted absorbers is graded to build in a small electric-field (~10^3V/cm) to facilitate transport into the depletion region. In a conventional p-i-n photodetecter the electron-hole pairs are generated in the i-region and travel in opposite directions. Since the overshoot velocity of electrons is much higher than the saturation velocity of holes, the i-region of a conventional p-i-n photodetecter is strongly influenced by the hole density. For the PDA photodiode, there is a p-doped absorber and an n-doped absorber on each side of the i-region. The p-doped absorber injects electrons into the i-region while the n-doped absorber injects holes. However, electron injection is much stronger than that of holes due to the different thickness of the absorber on each side. By proper design, the electron and hole currents can be tailored to greatly reduce the space charge effect, i.e., electron injection from the p-side into the i-region can balance the hole-dominated i-region.

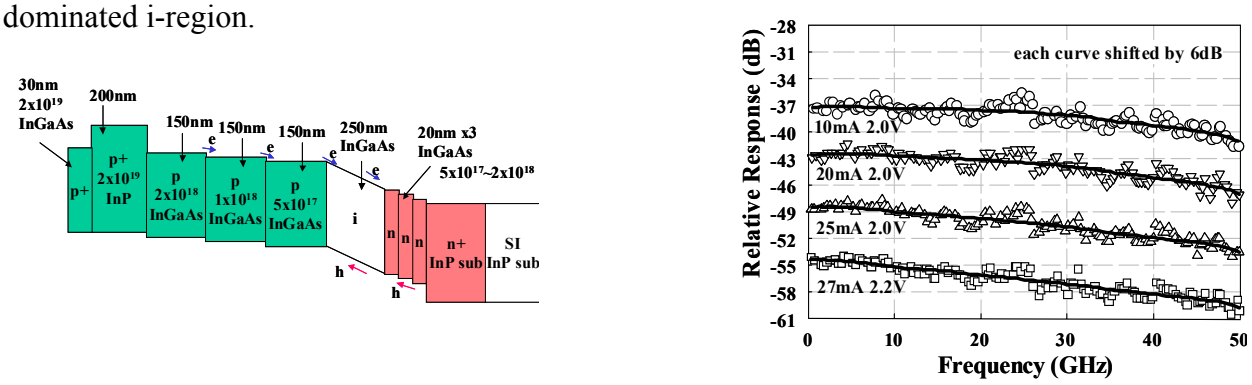

(a) (b)

Figure 2. (a) Partially-depleted-absorber photodiode structure. (b) Frequency response of 8 μm-diameter partially-depleted-absorber photodiode.

This new photodiode achieved a compression current of 27mA at 40 GHz, which yields a saturation current-bandwidth product >1000mA·GHz. An 18 μm-diameter device achieved an output power level of 10 dBm at 20 GHz (41 mA, 2.2 V). The PDA structure has achieved the highest current-bandwidth products reported to date for any photodetector.

In summary, new advances in overall link power efficiency are anticipated at higher data rates (>20Gb/s) with a combination of novel integrated laser-modulators capable of delivering relatively high output powers (> 10mW) at the transmitter side and high-saturation power photodetectors directly coupled to the electronic logic circuits at the receiver side. Electronic driver and receiver circuits identical to those being developed on longer distance on-chip electrical interconnects should be useable to avoid any further on-chip O/E interface electronics.

Efficient, Integrated Optical Transmitters for High-Speed Optical Interconnect Applications

Chad S. Wang[†], Erik J. Skogen[†], Gordon B. Morrison[†], James W. Raring[*], and Larry A. Coldren[†*]

[†]*ECE Dept. University of California, Santa Barbara, CA 93106*
[*]*Materials Dept. University of California, Santa Barbara, CA 93106*

Phone: 805.893.7065, Fax: 805.893.4500, Email: cswang@engineering.ucsb.edu

1. SUMMARY

For a variety of fiber optic data link, optical access, and computer interconnect applications, it is desired to have a coolerless, small-footprint, high-speed, high-efficiency transmitter in the 1300 – 1550 nm range. Chip to chip optical interconnects (C2OI) have the potential to demonstrate numerous advantages over traditional electrical I/O integrated circuits. Applications requiring high bandwidth-path length products will be best served through an optical free-space type interconnect [1]. This technology will also lead to advantages in power dissipation, crosstalk, and susceptibility to electro-magnetic interference (EMI) than electrical connections. Highly integrated transmitters would also be desired for low cost as well as the prospect of generating arrays of such elements.

In order to meet and exceed existing electrical I/O specifications, it is necessary to design and develop short cavity lasers with a small footprint (<250 μm pitch), high efficiency, low power dissipation, and high output power. Here we demonstrate a short cavity, high output power, single mode, high efficiency, distributed Bragg reflector (DBR) laser, monolithically integrated with an electro-absorption modulator (EAM). The devices were fabricated in the InGaAsP/InP material system and exhibited both good static and dynamic characteristics.

The short-cavity DBR lasers were designed to have a high-reflectivity (HR) rear mirror, short gain section (150 μm), and front DBR mirror (40 μm). The DBR lasers were monolithically integrated with an optional semiconductor optical amplifier (SOA) (75 & 110 μm) and EAMs (75 – 175 μm) using a quantum well intermixing processing platform that allows for the formation of a unique quantum well band edge for each integrated component. With this process it is possible to achieve any number of band-edges across the wafer, limited only by the practical number of lithographic process steps as shown in Fig. 1a and 1b. Therefore, each component of the device can be tailored for optimum performance. For this work, three band-edges were needed: the as grown band-edge for the gain regions (λ_{pl} = 1540 nm), a band-edge ideal for the EAM (λ_{pl} = 1500 nm), and a band-edge used in the low loss passive waveguide regions (λ_{pl} = 1430 nm). The photoluminescence curves for the band-edges used in this work are shown in Fig. 1c. The epitaxial base structure and fabrication details are given in Ref. 2. Fig. 2 illustrates this integrated laser-modulator.

The devices demonstrated both good static and dynamic characteristics. A low threshold current of 7 mA was measured, and output powers greater than 10mW were achieved with a gain section current of 30 mA, as shown in Fig. 3a. The wall plug efficiency exceeded 18%. The DBR lasers also demonstrated single-mode emission at 1543 nm with a SMSR greater than 40 dB, as shown in Fig 3b. The DC modal extinction characteristics of a 125 μm long EAM are presented in Fig. 3c. Greater than 20 dB optical extinction was measured at a reverse bias of 4 V. Modulation bandwidths were measured to be 25 GHz, and open eye diagrams were achieved at 10 Gbit/s NRZ bit patterns, as shown in Fig. 4a and 4b.

A first-generation of small footprint, high power laser-modulator devices have been designed, fabricated, and tested. The devices employed a QWI-based processing platform for the monolithic integration of multiple section photonic integrated circuits. Lasers exhibited excellent characteristics in terms of output power (>10 mW) and wall plug efficiency (>18%). The modulator demonstrated >20 dB DC extinction at a length of 125 μm, with 3 dB bandwidths up to 25 GHz. Taken together, the next generation of long-wavelength efficient transmitters will be implemented into arrays with vertically coupled output emission. Efficient transmitters in the 980 nm and 1300 nm wavelength range are also beginning to be explored.

2. REFERENCES

[1] M. R. Feldman, S. C. Esener, C. C. Guest, and S. H. Lee, "Comparison between optical and electrical interconnects based on power and speed considerations," *Applied Optics*, vol. 27, pp. 1742-1751, 1988.

[2] E. J. Skogen, C. S. Wang, J. W. Raring, G. B. Morrison, and L. A. Coldren, "Small Footprint, High-Efficiency, Integrated Transmitter for High-Speed Optical Interconnect Applications," *to be published at Integrated Photonics Research Conference* 2004.

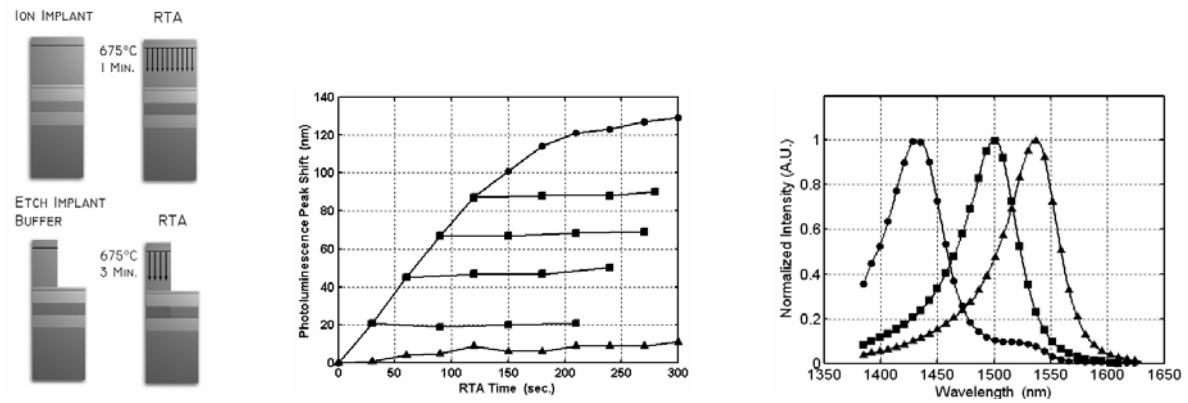

(a) (b) (c)

FIGURE 1. (a) Illustration of the intermixing processing platform used in this work. (b) Peak photoluminescence peak shift as a function of anneal time, showing the initial linear increase in the peak shift and the complete halting of the peak shift for samples for which the implant buffer layer has been etched. Symbols indicate non-implanted (triangles), implanted (circles), and samples with partial anneal followed by the removal of the implant buffer layer (squares). (c) Photoluminescence spectra for device shown in this work. Symbols indicate active region photoluminescence (triangles), EAM photoluminescence (squares), and passive section photoluminescence (circles).

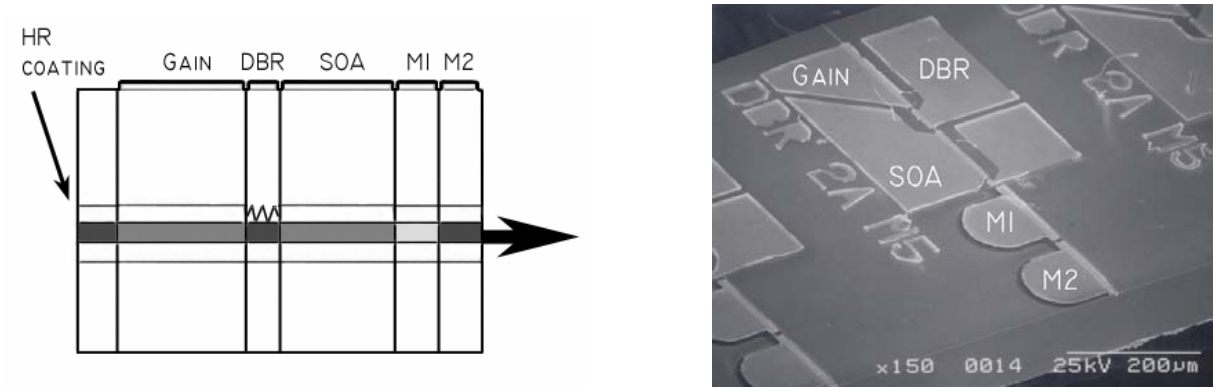

(a) (b)

FIGURE 2. (a) Side view schematic and (b) electron micrograph of the completed short-cavity DBR laser, illustrating the Gain, DBR, optional SOA, and 2-section EAM. This QWI platform takes advantage of the capability to integrate multiple band-edges across different sections of the device.

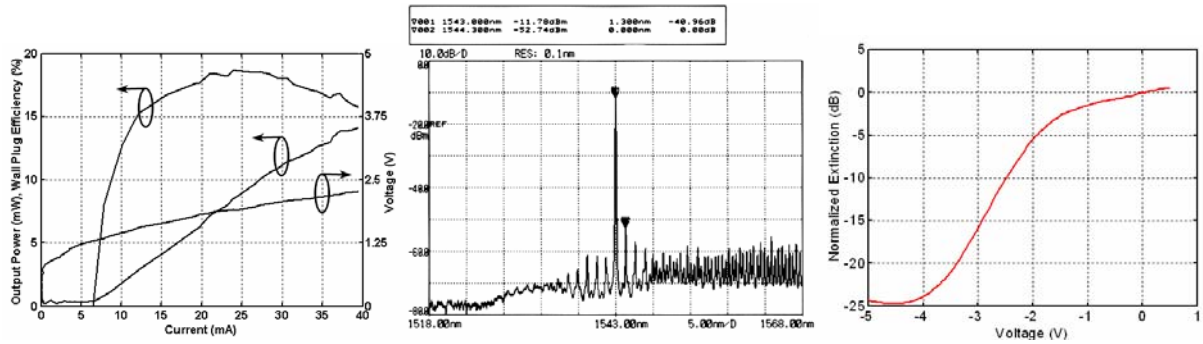

(a) (b) (c)

FIGURE 3. (a) LIV and wall plug efficiency under pulse testing. (b) CW lasing spectra showing emission at 1543 nm with greater than 40 dB SMSR. (c) DC optical extinction of a 125 µm modulator M1.

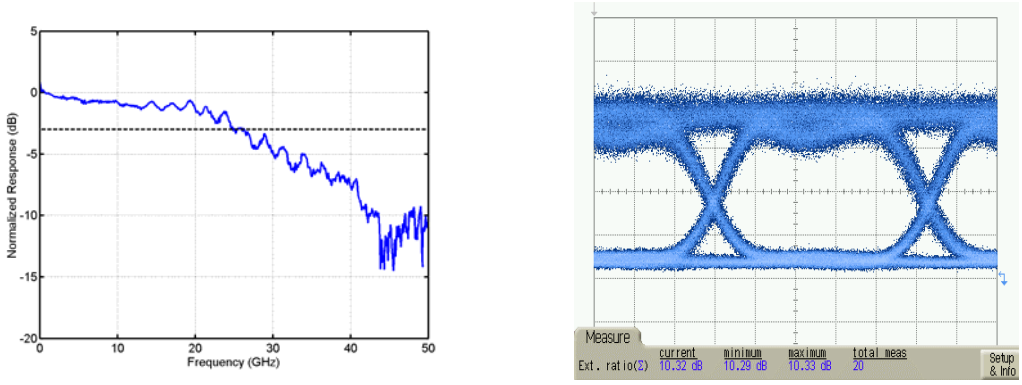

(a) (b)

FIGURE 4. (a) Modulation bandwidth of integrated DBR laser with 125 µm long modulator, showing 3dB bandwidth of 25 GHz. (b) Open eye diagram for 10 Gb/s transmission.

Monolithically integrated 40GHz pulse source with >40nm wavelength tuning range

L.A. Johansson, Zhaoyang Hu, D.J. Blumenthal and L.A. Coldren
Department of Electrical and Computer Engineering, University of California, Santa Barbara, CA 93106.
Email: leif@ece.ucsb.edu, Tel:(805) 893 2875, Fax: (805) 893 4500

Y.A. Akulova and G.A. Fish
Agility Communications, Inc., 475 Pine Ave, Santa Barbara, CA 93117.

Abstract: A monolithically integrated device combines 40 GHz dual mode-locked operation with the wide tuning range (>40nm) of sampled-grating DBR lasers, while further being integrated to an SOA and a potentially high-speed modulator.
OCIS codes: (250.5300) Photonic integrated devices; (140.3600) Lasers, tunable; (140.4050) Mode-locked lasers

1. Introduction

High-speed optical communications systems with transmission rates of 40 Gbps have been developed for future wavelength multiplexed high-capacity systems. One key enabling component, not previously demonstrated, is an integrated, wavelength-agile return-to-zero (RZ) optical pulse source. Although several integrated configurations have been reported in the literature to generate 40 GHz RZ pulse sources [1-3], none have been widely wavelength tunable. The topic of this paper is to demonstrate, for the first time, a single monolithically integrated device combining generation of spectrally compact RZ pulses with the wide tunability offered by an SG-DBR laser integrated with a semiconductor amplifier and an electroabsorption modulator. The modulator is at this stage not sufficiently fast for 40Gbps data encoding. However, MZ modulators integrated with widely tunable SG-DBR lasers, sufficiently fast for 40Gbps data encoding have recently been built and can be integrated with the dual-mode-locked laser.

In an extended perspective, this device would be well suited for integration to form a 40Gbps RZ transmitter. A conventional 40Gbps RZ transmitter typically consists of several optical and electrical components, including an optical source, two external modulators and drivers; one for pulse carving and one for encoding, and additional optical amplification, illustrated by Fig. 1a. The type of monolithically integrated device presented here has the potential to replace the majority of components in an RZ-transmitter, as indicated by Fig. 1b. This proposed transmitter would consist of a dual-mode-locked widely-tunable SG-DBR laser integrated with a semiconductor amplifier and a high-speed data encoder. Because the clock-reference is used only to synchronize the two modes, not to drive a modulator, the clock drive amplifier can in principle be eliminated.

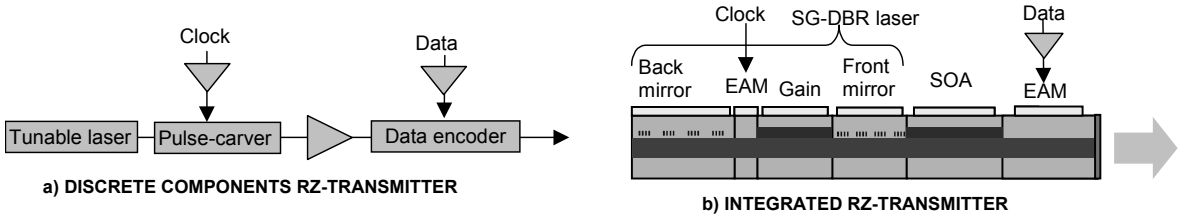

Fig. 1. a: Schematic of conventional wavelength tunable RZ optical transmitter. b: Schematic of proposed monolithically integrated RZ optical transmitter.

2. Experiment

The device used for this demonstration is the same as described in greater detail in reference [6]. It is based on a widely tunable sampled grating (SG) DBR laser with the structure shown in Fig 1b. The SG-DBR laser includes gain and phase sections positioned between two "sampled grating" distributed reflectors, sampled at different periods such that only one of their multiple reflection peaks can coincide at a time. An offset quantum-well structure provides a platform for integration of the laser with other active regions, such as detectors or semiconductor optical amplifiers (SOA), and passive regions, such as phase or amplitude modulators. Typical performance of an SG-DBR laser integrated to an SOA is more than 20mW fiber-coupled output power, lower than 2MHz linewidth, lower than

–140dB/Hz RIN and more than 40dB sidemode suppression ratio over more than 40nm wavelength tuning range. Also integrated in the device used in these experiments is an EA modulator designed for 2.5Gbps operation.

The sampled grating mirrors are designed so that only one single stable axial mode can be supported at a time. Mode-jumps between axial modes can be achieved by tuning the phase section, and at the mode boundary unstable operation is observed due to mode competition. By reverse biasing the phase section, it will take the function of an intracavity Franz-Keldysh modulator. Phase control must then be achieved by a combination of mirror and gain section tuning. A stable and synchronized dual-mode operation can be generated by modulating the phase section at the axial mode spacing frequency. Although the phase section has not been designed for efficient modulation at 40 GHz, the response is at the axial resonance sufficiently strong to correlate and stabilize the two lasing modes. In principle, if a high-speed modulator section is integrated in the laser, a much weaker drive signal can be used than for driving the equivalent external modulator, as only a small modulation is required to achieve mode synchronization.

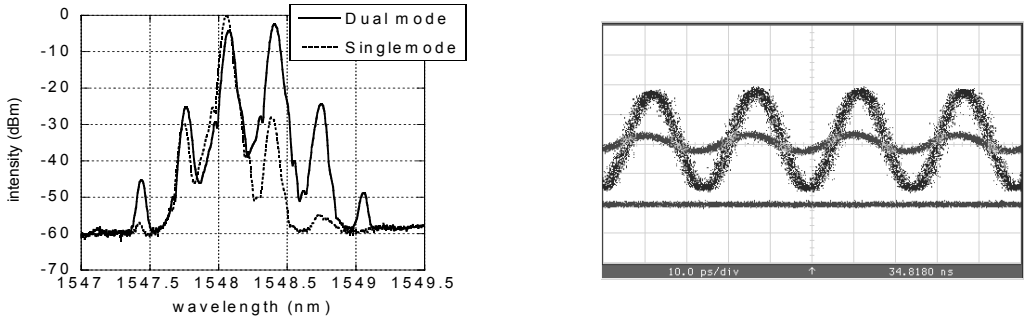

Fig. 2. a: Optical spectra for single and dual mode operation. b: Captured oscilloscope waveforms contrasting 40GHz dual-mode-locked and modulated single-mode SG-DBR laser operation.

3. Results

The optical spectra in Fig. 2a contrasts single and dual-mode operation under phase section modulation by a 19.3dBm signal. At single mode operation, weak modulation sidebands can be generated when the drive frequency matches the axial mode spacing; ~0.32nm. Adjusting the cavity round-trip phase, stable and synchronized dual-mode operation is observed. Figure 2b shows the comparison between the detected 40GHz waveforms generated under modulated single-mode and locked dual mode operation. The zero-level is also shown in the figure. At single-mode operation, a weak sinusoidal waveform was observed and it demonstrates that 40GHz optical pulses cannot be generated directly through strong modulation; while at locked dual-mode operation, a strong beat signal is obtained as a result of the heterodyne beat between the two locked modal frequencies. Based on the observed oscilloscope waveform, zero level, and the frequency roll-off of the 50GHz detector and 50GHz sampling oscilloscope used for detection, it is estimated that the actual extinction ratio is better than 10dB under dual-mode lasing.

The mode-beating can be synchronized over a 0.9GHz locking range, centered around 40.2GHz, corresponding to the cavity mode spacing of these devices, and illustrated by Fig. 3. At the boundaries of the locking range, a penalty in signal power was observed due to unbalanced mode amplitude. The 1-dB frequency range was on the order of 300MHz.

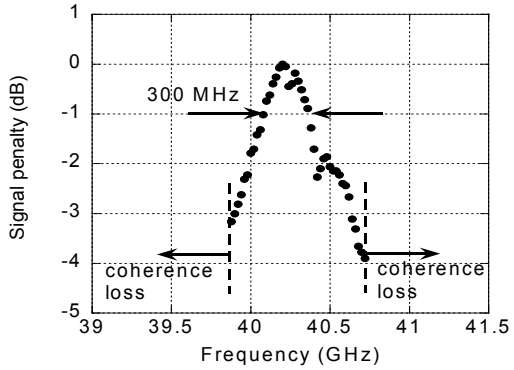

Fig. 3: Measured mode-locking range, where synchronized dual mode operation can be obtained. Also indicated is the 1-dB frequency range.

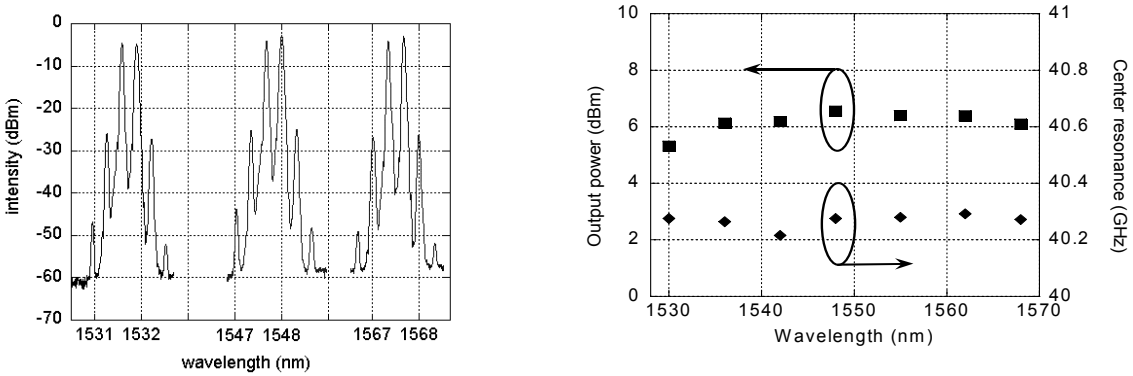

Fig. 4. a: Optical spectra taken through the tuning-range of the laser; low, center and high wavelength, illustrating a sidemode suppression ratio better than 20dB. (Res. bandwidth ~0.08nm). b: Fiber-coupled output power and center cavity resonance frequency over the wavelength tuning range of the laser.

Stable dual-mode lasing is obtained over the entire tuning-range of the laser; >40nm, illustrated by Fig. 3b, where dual-mode optical spectra at low, center and high wavelength are shown. The sidemode suppression ratio is at all wavelengths better than 20dB at a spectrum analyzer resolution bandwidth of ~0.08nm. The mode spacing remains well within the 1-dB lock-frequency range of Fig.3 over the wavelength tuning range of the laser, as shown in Fig. 4b, and is equally insensitive to chip operating temperature. The relative stability of generated modal beat frequency would allow the design of a widely-tunable dual-mode mode-locked laser for 40.0GHz or 42.7GHz applications. The fiber-coupled output power over the wavelength tuning range is consistent to that of single-mode operation and is also shown in Fig. 4b, where the gain section and SOA are kept at constant bias current.

4. Summary

In this paper we have demonstrated, for the first time, a single monolithically integrated device that combines generation of spectrally compact 40GHz pulses with wide wavelength tunability. This has been achieved by locking two axial modes of a widely-tunable SG-DBR laser to an external 40GHz reference used to modulate the reverse-biased phase section of the laser. The device is integrated with an SOA and an EAM that could potentially be designed sufficiently fast for data encoding, which would then be the realization of an integrated 40Gbps RZ transmitter. 40.2GHz pulse-generation is demonstrated with 0.9GHz locking range and uniform performance over the entire 40nm tuning range of the laser.

5. References

[1] C. Bobbert, J. Kreissl, L. Molle, F. Raub, M. Rohde, B. Sartorius "Novel Compact 40GHz RZ-Pulse-Source based on Self-Pulsating PhaseCOMB Lasers," *in Optical Fiber Communication Conference on CD-ROM (Optical Society of America, Washington, DC, 2004),* WL5.

[2] C. Bornholdt, B. Sartorius, S. Schelhase, M. Möhrle, and S. Bauer, "Self-pulsating DFB-laser for all-optical clock recovery at 40 Gb/s, " *Electron. Lett.,* vol. 36, pp. 327-328, 2000.

[3] K. Sato, A. Hirano, N. Shimizu, T. Ohno, and H. Ishii, "Dual mode op-eration of semiconductor mode-locked lasers for anti-phase pulse gen-eration," in *Proc. OFC 2000*, 2000, Paper ThW3.

[4] Y. A. Akulova, G. A. Fish, P. C. Koh, C. Schow, P. Kozodoy, A. Dahl, S. Nakagawa, M. Larson, M. Mack, T. Strand, C. Coldren, E. Hegblom, S. Penniman, T. Wipiejewski, and L. A. Coldren, "Widely-Tunable Electroabsorption-Modulated Sampled Grating DBR Laser Transmitter", *IEEE J. Selec. Top. in Quantum Electron.*, vol. 8, pp. 1349-1357, Nov/Dec 2002.